Fall 12-2020

Detailed Modeling of the Flash Hydrolysis of Algae for Biofuel-Production in COMSOL Multiphysics

Noah Joseph LeGrand
Old Dominion University, NLEGR001@ODU.EDU

DETAILED MODELING OF THE FLASH HYDROLYSIS OF ALGAE FOR BIOFUEL -PRODUCTION IN COMSOL MULTIPHYSICS

by

Noah Joseph LeGrand
B.S. May 2019, Old Dominion University
M.S. December 2020, Old Dominion University

A Thesis Submitted to the Faculty of
Old Dominion University in Partial Fulfillment of the
Requirements for the Degree of

MASTER OF SCIENCE

MECHANICAL ENGINEERING

OLD DOMINION UNIVERSITY
December 2020

Approved by:

Orlando M. Ayala (Director)

Robert L. Ash (Co-Advisor)

Sandeep Kumar (Member)

Xiaoyu Zhang (Member)

ABSTRACT

DETAILED MODELING OF THE FLASH HYDROLYSIS OF ALGAE FOR BIOFUEL -PRODUCTION IN COMSOL MULTIPHYSICS

Noah Joseph LeGrand
Old Dominion University, 2020
Director: Dr. Orlando M. Ayala

Algae-derived biofuels are being commercialized as an important renewable energy source. Like any new technology, conversion improvements are desired, including reductions in process complexity and better utilization of the entire microalgae feedstock. The Old Dominion Biomass Laboratory has focused on flash hydrolysis for algae biofuel production. That process involves rapidly heating algae and water mixed as a slurry to a subcritical state. Results from small-scale bench tests are promising, but process scale up is a challenge. Currently there exists a pilot laboratory scale system utilizing induction heating in order to reach controlled reaction temperatures with a reaction duration of 10 seconds or less. However, the influence of the induction heating process on the resulting reactions had not been examined. That is the focus of this thesis.

The pilot flash hydrolysis reactor system has been simulated utilizing COMSOL Multiphysics 5.1. The COMSOL model assumed fully developed laminar slurry flow with an electromagnetic field, rate sensitive chemical reactions, and diffusive transport of dilute species. Mesh refinement analysis, mass and energy balances, and experimental verification have been utilized to validate the model. This study has shown that industrial scale up challenges will include sensitivity to feedstock channel size, induction coil pitch, length and excitation

frequency, process residence time, and algae concentration. Furthermore, process efficiency improvement may be possible by thermal management of the rapid heating and subsequent quenching process.

This thesis is dedicated to the many scientists, activists, and engineers working tirelessly for a better tomorrow. Your dedication motivates me.

ACKNOWLEDGMENTS

There are many people who have contributed to the successful completion of this thesis. I cannot thank my director, Dr. Orlando M. Ayala, enough for his patience and the many hours he spent guiding me and reviewing my work. Dr. Ayala's commitment to this work and to its success has been inspiring. I would also like to thank Dr. Robert L. Ash for his time spent advising me and reading my manuscript to improve it. Dr. Ash has always believed in me and is a large part of why I was sure that I could succeed in my graduate education and for that I will always be thankful. Dr. Sandeep Kumar and Dr. Xiaoyu Zhang also deserve recognition for their contribution to this work; they have both played an integral part in my education. I would also like to thank my family, friends, and classmates for their support during this time of my life, which I will always remember fondly.

NOMENCLATURE

A	Forward Frequency Factor (Response Time Rate)	m^3/mol-s
$\bar{A}$	Magnetic Vector Potential	T-m
A_c	Area of Coil	m^2
B	Magnetic Flux Density	T
c	Concentration	mol/m^3
C_p	Specific Heat Capacity at Constant Pressure	J/kg-K
d	Diameter	m
D	Pipe Diameter	m
D_i	Diffusion Coefficient	m^2/s
E	Activation Energy	kJ/mol
F	Volumetric Flow Rate	m^3/s
Gr	Grashof number	
H	Magnetic Field Intensity	A/m
h	Heat Transfer Coefficient	W/K-m^2
I	Current	A
I	Identity Matrix	
j	Imaginary Number	
J_e	External Current Density	A/m^2
k	Rate Constant	m^3/mol-s
L	Length of Reactor	m
L_c	Length of Coil	m
$\bar{m}$	Mass Flow Rate	kg/s
M	Molar Mass	
$\vec{n}$	Normal Unit Vector	

Nu	Nusselt Number	
p	Pressure	Pa
P	Power	W
P_d	Phase Volume Fraction	
q	Heat Flux Vector	W/m^2
Q	Heat Source	W/m^3
r	Reaction Rate	$mol/s\text{-}m^3$
R	Resistance	Ω
$\bar{R}$	Universal Gas Constant	J/mol-K
R_i	Chemical Reaction Rate Equation	1/s
r_p	Radial Coordinate	m
R_p	Radius of Reactor	m
Ra_L	Rayleigh number	
Re	Reynolds number	
Stk	Stokes Number	
T	Absolute Temperature	K
t	Time	s
u	Velocity	m/s
U_c	Velocity of Continuous Phase	m/s
V	Volume	m^3
V_{avg}	Average Velocity	m/s
x	Species Conversion	
ε	Electric Permittivity	
λ	Thermal Conductivity	W/m-K
μ	Dynamic Viscosity	Pa-s
μ0	Magnetic Permeability of Free Space	
ρ	Density	kg/m^3

ρ_e	Electrical Resistivity	
σ	Cauchy Stress Tensor	
ω	Radial Frequency	Hz

TABLE OF CONTENTS

Page

Page

LIST OF TABLES

LIST OF FIGURES

Figure Page

CHAPTER 1

INTRODUCTION

1.1 Background

With the depletion of fossil fuels and the global rise of carbon emissions, the need for green energy and biofuels has never been greater. However, the struggle has always been to not only make the technology economically viable, but also allow for potential cost savings or other added benefits. The energy industry is embracing the conversion to clean and sustainable fuels, with companies like Exxon currently using algae to produce biofuels commercially. Currently, catalytic breakdown of algae is followed by lipid separation and subsequent fuel post-processing. The catalytic chemical process creates unusable waste. Since microalgae consists primarily of proteins and carbohydrates that when isolated economically can be just as valuable as the lipids, alternate process strategies should be considered.

Dr. Sandeep Kumar of Old Dominion University (ODU) has worked to develop a flash hydrolysis method for lipid extraction from biomass as a cleaner alternative to the catalyst reaction [1]. Flash hydrolysis utilizes a rapidly heated algae water slurry to fractionate the algae into its chemical components so that each can be recovered and potentially utilized. However, the temperatures needed to initiate and sustain the reaction are in the range of 250-320 ^{o}C and the slurry must remain in the liquid phase to permit the hydrolysis reaction to occur. The slurry reaction pressure must be between 1500-2000 psi (100 and 140 atm.), slightly above the vaporization pressure for water at these temperatures. This is also considered to represent an acceptable upper pressure limit for safe operation of commercial equipment. The ODU flash hydrolysis system works well at benchtop laboratory scales but is not easily scaled up to

industrial scales due to inefficient heating and small diameter tubing issues limiting high concentration algae and water slurries. To address these issues, Dr. Ayala and Dr. Kumar oversaw a pilot scale system design that was fabricated at ODU with the help of a student team. The pilot scale design incorporates an adjustable flow, piston-driven pump, and an induction heater capable of 5 kW of energy to heat a continuous flow of water and algae to controlled temperatures. The induction heater is controlled by a PID controller that ramps up the applied induction coil power to elevate the water temperature to the desired reaction temperature as it is combined with algae feedstock, creating the temperature-controlled slurry. The slurry is then cooled and depressurized with a back-pressure regulator. This has proven to be a capable design for optimizing the reaction parameters, but it is a very energy intensive process. Previously, the modeling related to this flash hydrolysis process has been reaction based; namely reaction kinetic modeling for determining the best reaction temperature and residence time, which is the time the algae and water slurry spends in the reactor. However, computational fluid dynamics (CFD) and finite element analysis (FEA) can incorporate all of the major phenomena in the pilot scale reactor. In that way, system development can be guided toward the efficiencies expected for large-scale use in industry.

1.2 Statement of Work and Objectives

The goal of this research was to model flash hydrolysis in a pilot scale reactor utilizing COMSOL Multiphysics 5.1. Modeling starts with a simplified process initially and then adds complexity until its performance closely approximates the real process in the lab. This finished model can then be used to predict system changes to guide redesign efforts for better performance. The model was validated utilizing several different COMSOL examples and

published literature case studies, adding the various physical processes one by one until the model is complete. There are five different physical processes needed to sufficiently model this system, including laminar flow, heat transfer, magnetic fields, transport of diluted species, and chemical reactions. Time spent with the system leads to understanding how it works and designing test cases to verify the model. Resources such as online COMSOL lectures and even communicating with the companies that provided the components of the system provided clarity on the correct and efficient way to model the system. The model was fine-tuned through small adjustments to the model parameters and the validity of the results have been checked through mesh refinement and mass and energy conservation balances. Once the overall model was completed, a parameter sensitivity analysis was run to see how the reacting flow changes with alterations in several key parameters that are thought to make a difference. One goal was to outline a design iteration strategy to facilitate system improvements.

1.3 Literature Review

The Old Dominion Biomass Laboratory report on flash hydrolysis of microalgae was by Garcia-Moscoso, Obeid, Kumar, and Hatcher in 2013 [1]. The idea is simple: heating up algae, in this case Scenedesmus sp., and water in the subcritical phase allows the various reactions to be controlled and manipulated so that the algae can be broken up into several useful products. Microalgae is mostly proteins, carbohydrates, lipids, and ash. Therefore, if each component can be extracted effectively, algae can become an even more valuable biomass. The conceptual challenge is each component has different reaction kinetics requiring precise temperature and reaction time control in order to control the algae fractionation, optimizing product extraction. No continuous flow system had been used to fractionate algae before Dr. Sandeep Kumar's

research in 2013, so hydrolyzing to segregate the proteins from the algae while keeping the lipids for biofuels was an important breakthrough [1]. To take it a step further, flash hydrolysis can be manipulated to increase bio-crude oil production to levels greater than the original lipid content because proteins can also be broken down and reformed into biofuel intermediates [2]. Flash hydrolysis differs from most hydrothermal liquefaction reactions by enabling much shorter reactions, or residence times. Faster is better for bio-crude yield, since flash hydrolysis produces yields that are greater than the general hydrothermal liquefaction [2].

Recently, Norazalia Jamil [3] developed a mathematical model for high concentration suspensions of lignocellulosic biomass undergoing hydrolysis utilizing enzymes. Her model is comprehensive but is focused specifically on suspensions of lignocellulose and does not translate readily to algae processing because the derivation assumes small rod-shaped feedstock material. A major takeaway from the model is that mixing is a critical aspect in controlling and predicting reaction uniformity [3]. Another study modeled biofuel production from cellulose using a batch reaction process [4]. They concluded the temperature cycle was a major factor in controlling the reaction in a batch process because it produced a sample with two different products determined based on whether the temperature cycle approximated a ramp or rapid step function like variation [4].

More recently, the influence of temperature, residence time, flow rate, and heating rate were studied for algae undergoing hydrothermal liquefaction in a plug-flow reactor [5]. In general, the researchers found that steadily increasing reaction temperatures between 300 and 380 ^{o}C reduced the water-soluble products of the reaction, and the ideal residence time for the water-soluble products was approximately one minute [5]. While much can be learned from

these studies, no serious attempt has been made to model systems similar to the Old Dominion Biomass Laboratory continuous-flow flash hydrolysis reactor.

The Old Dominion Biomass Laboratory has employed Scenedesmus sp. algae in their flash hydrolysis studies. The composition of the Scenedesmus sp. algae by components is displayed as (Figure 1). The Biomass Laboratory reported that if the flash hydrolysis was treated as a single step reaction it would generally follow the following process:

Algae + Water → Peptides + Amino Acids (Arginine) + Sugars (Glucose) + Biofuel Intermediates + Others (Gas, etc.)

A molecular reaction equivalent for flash hydrolysis of Scenedesmus sp. algae can be represented:

$$4.48C_1N_{0.160}H_{1.877}O_{0.387} + 0.9H_2O \rightarrow 1.26C_1N_{0.203}H_{1.778}O_{0.382} + 0.02C_6H_{14}N_4O_2 + 0.07C_6H_{12}O_6 + 2.32C_1N_{0.093}O_{0.245} + 0.5C_{0.76}H_{2.39}O_{0.63}N_{0.36} \quad \text{(Eq. 1)}$$

While this reaction is representative of the overall process, it lacks specificity regarding the actual chemical reaction sequences. Actually, multiple independent reactions are occurring simultaneously. However, modeling all the different reactions is challenging because algae is not a single molecule and the various components react at different rates [2]. The flash hydrolysis algae reaction of primary interest is the fractionation of proteins into soluble peptides because they are valuable byproducts. Their removal from the bio-crude solution would eliminate the

need to extract them prior to final biofuel production. Proteins make up 54% of Scenedesmus sp. Microalgae by mass, of which Arginine makes up 16% [6].

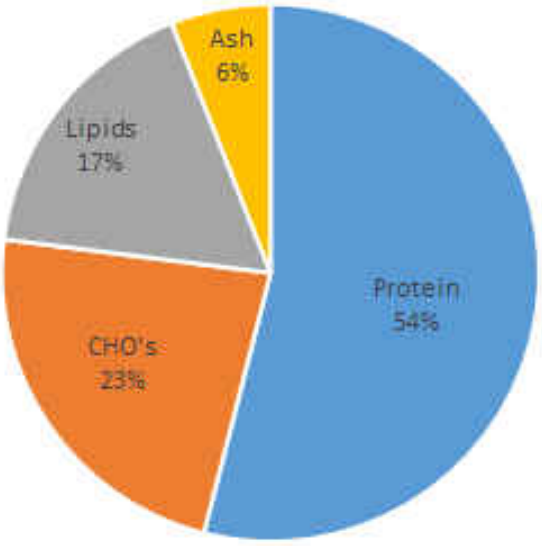

Figure 1. Scenedesmus sp. chemical composition [6]

Because the algal protein is of interest, the ODU-team has studied the reaction kinetics, which determines when and how the hydrolyzation of proteins and arginine within the proteins occur. Arginine was observed as the main free amino acid reaction in the hydrolyzate [6]. That analysis was completed with the laboratory scale benchtop unit at Old Dominion University. From that analysis a model for the reaction was developed using the Arrhenius Law.

$$k = A \cdot e^{\frac{-E}{RT}} \qquad \text{(Eq. 2)}$$

In Equation 2, the forward frequency factor (A), rate constant (k), and activation energy (E) are obtained from experimental measurements while absolute temperature (T) and the universal gas constant ($\bar{R}$) are standard symbols. The activation energy is the energy required for the reaction to occur. The forward frequency factor, otherwise known as the response time rate, indicates frequency of the collisions of the molecules involved in the reaction. Based on these factors, the rate constant is a measure of how quickly the reaction will proceed independent of the concentrations of reactants. Using three reaction temperatures, a kinetic model was developed employing the parameters in Table 1 [6].

Table 1. Kinetics of flash hydrolysis of Scenedesmus sp. [6]

	Proteins	Arginine
Activation Energy (kJ/mol)	43.01	34.31
Forward Frequency Factor (m^3/mol*s)	81.534	1.112
Reaction Order	2	0

The concentration-based reaction rate is then just a product of the rate constant and the concentration of the reactants to the power of the reaction order based on the specific reactant (Eq. 3). Reaction order indicates how the concentration affects the rate exponentially. Excess water was assumed in the kinetic study, so the reaction rate equations do not depend on the concentration of water. The reaction rate equations for proteins and arginine are as follows:

$$r_{proteins} = k_{proteins} \cdot \left[C_{proteins}\right]^2 \qquad \text{(Eq. 3)}$$

$$r_{arginine} = k_{arginine}$$

The reaction rate of proteins is a quadratic function of their concentration while the arginine is zeroth order meaning concentration does not affect it.

A case study was presented in a chemical engineering textbook [7] demonstrating how to incorporate similar reactions in CFD and FEA codes; that case study modeled the hydrolysis of propylene oxide in a reactor with axial and radial concentration variations. It assumed the reaction occurred with excess water and therefore water availability was not a variable and did not affect the rate equations; gradient-based molecular diffusion influences were therefore neglected. In addition, a cooling jacket surrounded the reactor slowing the reaction rate at the wall. That case study provided a blueprint for the modeling reactions in which axial and radial variations in temperature occurred.

In this research the water is modeled as a solvent, which implies several restrictions in COMSOL including requiring the physical properties for the mixture to be the same as water unless otherwise specified; and the convective term in the flux of species, which dictates how the chemical species are transported, is solved by multiplying the flow velocity by the algae concentration. With reference to the heat of reaction for the flash hydrolysis of algae, which is the change in enthalpy due to the chemical reaction, there is no directly relevant literature on these short residence time reactions for specific algae species. Some literature studying hydrothermal liquefaction of microalgae reported that the heats of reaction range from mildly endothermic to mildly exothermic [8]. On that basis, it is reasonable to assume as a first approximation that the heat of reaction can be neglected.

CHAPTER 2

EXPERIMENTS AND MODELING

2.1 Experimental Setup

Flash hydrolysis of algae has been carefully developed in a laboratory setting for over a decade [1]. Two experimental designs have been engineered and maintained in working order; both will be characterized in this section.

2.1.1 Laboratory Scale Apparatus

The original laboratory scale unit utilizes two high pressure water pumps to propel the algae slurry through the reactor. The first pump directly drives pure high-pressure water through the electric furnace to preheat it before it mixes with the concentrated algae slurry stream that is introduced employing the second pump, pressurizing the algae slurry. The water and concentrated algae then mix to form a 1% algae-to-water mass ratio slurry flowing back into the electric heater where the reaction occurs. Subsequently, the mixture is rapidly cooled through with a heat exchanger and depressurized to atmospheric pressure employing a back-pressure regulator, as diagrammed in Figure 2 [1].

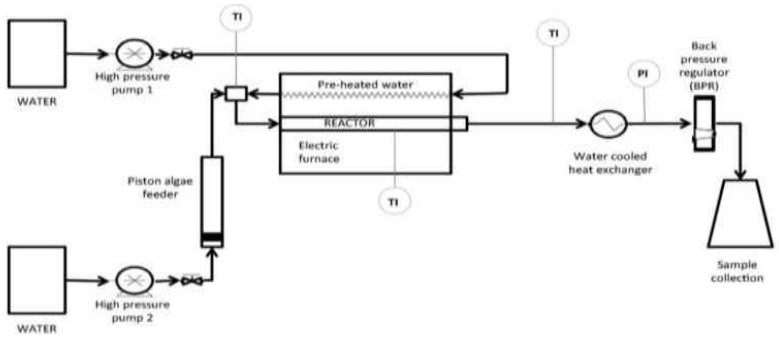

Figure 2. Schematic diagram of the lab scale flash hydrolysis design [1]

While this design has proven quite useful for proof of concept and associated studies, it is not easily scaled up to a size and production capability that could establish economic feasibility for industrial purposes. Several areas must be addressed in order to improve the production and justify the product cost including: increasing the mass ratio of algae-to-water; decreasing the process time; adequately mixing the concentrated algae slurry at a higher flow rate; and supplying the heating required for the reaction in a more efficient and scalable manner. The algae slurry weight percentage is particularly important because the initial investment costs and operating cost both decrease by nearly a factor of two when comparing a 5% wt. slurry to a 20% wt. slurry [9]. Clearly a higher concentration of algae would be preferable.

2.1.2 Mobile Pilot Unit

The *pilot unit* was intended to address scalability of flash algae hydrolysis. A concentrated algae and water slurry is first mixed continuously prior to entering the pump. A single pump drives the flow: a piston-powered adjustable flow rate pump with performance exceeding the requisite reaction pressure (1500 psi). Subsequently, a pulsation dampener charged with pressurized nitrogen is utilized to reduce any pump-derived pressure fluctuations. The slurry flows through a 16 inch (406 mm) long reactor utilizing $^{5}/_{16}$ inch (7.9 mm) diameter stainless steel tube with ⅛ inch (3 mm) thick walls. The first 12 inches of the reactor is heated employing an internally water-cooled, 19-coil (1.6 coils per inch pitch) induction heater. The heater has ¼ inch (6.4 mm) square cross section coils. The heater is powered with a 5 kW AC power source employing a PID controller. The controller receives feedback from a thermocouple located at the reactor exit. The slurry product is then rapidly cooled and depressurized. Reactor

pressure is controlled employing a diaphragm-based back-pressure regulator. A schematic diagram of the setup as well as a picture of the system are provided in Figures 3 and 4 [10].

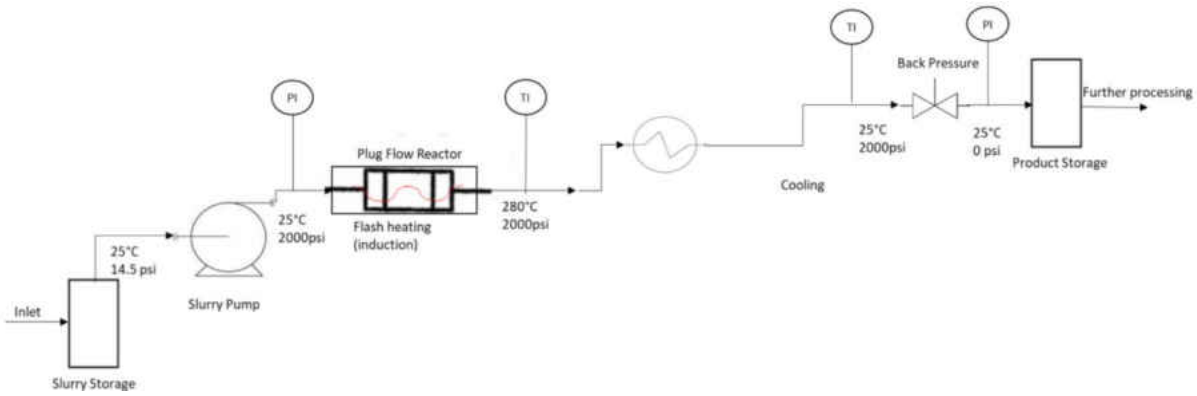

Figure 3. Schematic diagram of the pilot flash hydrolysis system [10]

Figure 4. Mobile algae processing pilot unit

The reactor in the mobile pilot unit was the focus of this modeling study. The design and fabrication of the mobile pilot unit is detailed elsewhere [10].

2.2 Physical Phenomena

The mobile pilot unit utilizes two-phase flow, induction heating, convection and radiation heat transfer processes while requiring reaction kinetics modeling. Key fundamental process elements are identified and discussed so that they can be understood before the details of the modeling procedure are discussed.

2.2.1 Viscous Flow in a Pipe

Fully developed laminar pipe flow is modeled relatively simply in COMSOL. The most important characteristic to note is the viscous no slip boundary condition. This zero velocity condition results in a fully developed parabolic laminar velocity profile within the pipe. In the mobile pilot unit, the target flow rate for the reaction to occur in 10 seconds was 95 mL/min, which through the $^{5}/_{16}$ inch diameter reactor tube equates to 3.2 cm/s average velocity. The Reynolds number for the flow of a 10% by mass algae to water slurry at 20 ºC is 265 assuming a mass-averaged slurry density of 1045 kg/m^3, where the density of the algae is a measured value as explained in the material properties section. A Reynolds number of 265 indicates that the flow is laminar so the velocity profile in cylindrical coordinates is:

$$u(r) = 2 \cdot V_{avg} \cdot \left(1 - \left(\frac{r_p}{R_p}\right)^2\right) \qquad \text{(Eq. 4)}$$

In Equation 4, u(r) is the velocity at a given radial position, V_{avg} is the average velocity of the flow, r_p is the radial position in the pipe, and R_p is the radius of the pipe.

2.2.2 Two-Phase Flow

Two-phase flows can exhibit separated phases, mixed phases, and dispersed phases [11]. Approaches for modeling micro two-phase flows vary based mainly on the volume and mass fractions of the particle and carrier phases, as well as several non-dimensional scaling parameters including Reynolds and Stokes numbers [12][13]. The algae-water slurry is modeled at a maximum of a 10% algae to water by mass. The volume fraction ratios were similar since the densities of water and algae are similar. Ten percent algae loading is the boundary of the dispersed phase; above that ratio individual particle velocities and momenta would need to be considered. The flow is definitively laminar which favors the dispersed phase assumption. The Stokes number is defined:

$$Stk = \frac{\rho_p \cdot d_p^{\,2} \cdot u_c}{d \cdot 18 \cdot \mu_c} \qquad \text{(Eq. 5)}$$

Assuming a particle density (ρ_p) of 1437.5 kg/m^3 (calculated at Old Dominion Biomass Laboratory), a range of particle sizes (d_p) from 35 to 425 μm, the continuous phase flow velocity (u_c), the diameter of the pipe (d), and a viscosity (μ_c) that ranged between 94.8 x 10^{-6} and 998 x 10^{-6} Pa-s, the Stokes number is in the range of 4 x 10^{-4} and 0.6 throughout the reactor [14]. A value less than one means that the particles will closely follow the fluid streamlines. The particles behave as a dispersed phase [13].

2.2.3 Induction Heating

Induction heating has been employed since the nineteenth century when induced electrical current was discovered. The process starts with an alternating current passing through a coil of conductive material. As the current alternates, it generates a magnetic field. When a conductive material is placed in that magnetic field, eddy currents are created in the material and heat is generated [15]. The induced current is governed by Ampere's Law.

$$\oint \vec{B} \cdot \vec{ds} = \mu_0 I \qquad \text{(Eq. 6)}$$

Here, B is the magnetic field, ds is the direction tangent of the coil, I is the current, and $\mu_0$is the permeability of free space. The energy released by the induced current is governed by the Joule effect.

$$P = I^2 \cdot R \qquad \text{(Eq. 7)}$$

The P represents power, I is current, and R is resistance.

The skin effect, in alternating current coils, concentrates heating on the outer surfaces. This is mirrored for heated work pieces where most of the energy is released through what is known as the penetration depth, through which 87% of the heat is generated [16]. This effect can be seen in the model as induction heating focuses on the outside of the pipe and only then is it conducted inwardly toward the slurry flow. As the pipe wall is heated, the process of heat transfer through the thermal boundary layer occurs. Close to the pipe wall, heat is conducted into

the nearly stagnant bounding fluid because of the no slip condition. Radial fluid motion is due only to the combination of density changes and associated flow redistribution.

Induction heating is a common model condition using FEA, where many studies have considered various induction heating applications. In 2011, a research team from Indonesia studied inductor plates to investigate the influence of plate thickness and plate inductor spacing on the heated workpiece and the current density [16]. While large differences based on the inductor thickness were not observed, likely attributable to the skin effect, the maximum current density decreased with increasing separation distance, even though the distribution of current density remained the same [16]. This result indicates that reductions in the gap between the inductor and workpiece is more desirable for fast heating. Another study on the theory of induction heating sought a mathematical model that could closely match FEA results [17]. This undertaking was impressive, but it focused on designing a mathematical model for a physical system requiring very accurate temperature profile measurements. In general, repeatable experimental temperature distributions within induction heated hardware elements do not exist presently. Thermocouples and infrared cameras are often used for verification, but even they have errors associated with measuring accuracy [18]. Considering these limitations, the accuracy of the model must be validated using several methods, which will be explored in the model validation section of this paper.

2.2.4 Reaction Kinetics Modeling

Flash hydrolysis of algae is actually many different small reactions occurring in parallel and series. With so many identifiable chemical products, it is very difficult to model each reaction process with any accuracy. One way to combat this problem is to simplify the analysis

by lumping products together and treating the reaction as elementary, where the reactants convert to products in one step. This also simplifies the reaction order since it is based on the coefficients in the reaction equation while removing specific physical and chemical phenomena from the rate equation [19]. This is a powerful method for studying reactions that have intermediate steps. Also, the method works well with experimental models created from data because any grouping of products can be analyzed to form a kinetic model. Transient experimental data can be correlated using the Arrhenius Law, as was described in Equation 2 in the literature review.

The lumped approach has its drawbacks, not the least of which is that the model does not account for the molecular processes required for the reaction to occur [19]. This could of course be a problem if the models are used improperly to predict reactions that are not in agreement with those originally modeled. There are a few other options for more detailed reaction modeling, such as mechanistic and molecular models. Mechanistic models focus more on the reaction pathways and molecular models involve analysis of the changes that each molecule type undergoes [19]. Both of these model types are generally considered upgrades over lumped analysis and should be considered in the future for the modeling of flash hydrolysis.

2.3 Assumptions

Perhaps the most impactful assumption made is that the entire reactor is modeled as axisymmetric about the centerline of the pipe flow. This assumption is consistent with the geometry of the reactor tube, but it is an approximation for the geometry of the induction coils. While the induction heater coil in the lab winds around the reactor tube without breaks, the model assumes each loop around the pipe to be continuous. However, the inductor coils are still modeled in series with each other electrically and the projected area that the inductor surrounds

the pipe is approximately equal. It is possible that if the inductor was modeled completely the helical geometry of the coils would induce a swirling flow with steadier temperatures because the entire length of the reactor would be heated along the circumference of the pipe. Further modeling research could explore such inconsistencies in this model. Presently, the axisymmetric assumption is quite reasonable, and it simplifies the modeling space while also reducing the computation time by orders of magnitude.

As far as the fluid flow is concerned, several other assumptions were made including the non-oscillating driven flow. In the lab, the pilot unit flow was pressurized using a single piston pump. A piston pump was the choice due to the high pressures needed to maintain the flow in the liquid phase at the desired temperatures. Piston pumps expand to draw in fluid and compress to pressurize it and utilize one-way valves to control the flow. Therefore, the pump only drives the flow in the compression stage. To combat this unsteady flow, a pulsation dampener charged with nitrogen and calibrated for the desired supply pressure is placed in the flow path immediately after the pump. The dampener fulfills its purpose and smooths the flow unsteadiness considerably, but a small amplitude pressure oscillation can be observed in the pressure gauges. For this research, the flow was considered to be steady. In future studies, a small amplitude oscillation function could be added to the model based on sampled pilot unit pressure data.

Another assumption was that the flow is weakly compressible, which allows the density to be calculated based on the local temperature. According to the COMSOL documentation in the help section of the laminar flow interface, incompressible flow means that the model bases the density on the reference pressure and temperature. With this model, the temperature is increased more than ten-fold which makes the density changes within the pipe due to the temperature significant. The weakly compressible flow option allows the model to keep up with

the density changes, as proven later in the mass conservation model check. Without this assumption, the large density variations would not be considered in the model. Furthermore, the flow is assumed to be a well-mixed slurry of algae and water, meaning that the algae particles resist clumping and are dispersed evenly throughout the flow. Also, convection is assumed to be the dominant transport mechanism for the algae, the algae and water were assigned very small diffusion coefficients (10^{-8} m^2/s) because no diffusion is expected to occur when the algae is still in the solid state. However, the products of the reaction are in part aqueous so COMSOL is left to calculate their diffusion coefficients considering the temperature, molecular weight, viscosity, and density of the products. The Wilke-Chang equation, gathered from the COMSOL documentation, is used for the calculated diffusion coefficients.

$$D_i = \frac{3.7 \cdot 10^{-15} T \sqrt{M_{solvent}}}{\mu_{solvent} \left(\frac{M_i}{\rho_i} \right)^{0.6}} \quad \text{(Eq. 8)}$$

Another simplification to reduce the computation time drastically is to model the heat transfer effects of the surrounding air and coil cooling water instead of modeling their entire fluid dynamics. The pipe surface included a heat flux boundary condition with a composite heat transfer coefficient that is calculated, as explained later in the non-COMSOL calculations section. Additionally, radiation cooling of the coil surroundings is estimated, while assuming a minimal natural convection heat transfer coefficient for the coils and cooling water on the inside surface of the coils based on the supply cooling water mass flow, heat capacity, and temperature difference. Further explanation on the calculations and selections can be found in later sections.

2.4 Material Properties

COMSOL maintains a suite of predefined materials. The present model has employed three predefined materials and one user-created material. Each material property was researched and modified for the purpose of this research. Copper was utilized as the coil material. The only nonstandard adjustment for air was its relative permittivity, utilizing a value of 1.0006 rather than unity [20]. Relative permittivity is the measure of the ease with which a material becomes polarized in the presence of a magnetic field compared with its vacuum value. Water required two additional properties: relative permittivity and relative permeability. Similar to permittivity, relative permeability is the measure of the ease with which a material becomes magnetized by a magnetic field compared with that of a vacuum. The relative permeability of water was set to unity [21]. Relative permittivity of water is a function of temperature. In COMSOL, functions can be defined by interpolation of tabulated data. Data for water at 10 MPa is available covering a suitable range of temperatures [22].

A new material was generated by modifying property data for AISI 4340 steel to match the material properties of 316 stainless steel for the reactor pipe. Relative permeability was adjusted from 1 to 1.0047 and relative permittivity was set equal to 4.5 [23] [24]. Density was taken to be 8238 kg/m^3. Temperature-dependent specific heat capacity and thermal conductivity were imported from tabulated data [25]. Electrical conductivity is a function of temperature based on data from the inverse of electrical resistivity [26]. Finally, the coefficient of thermal expansion for the 316 stainless steel was 16.0 x 10^{-6} 1/K based on several online resources [27]. Surface emissivities of 0.9 for the red painted copper coils and 0.5 for the partially wrapped reactor insulation [28].

The specific heat of the reacting flow was equivalent to the specific heat of water since water constituted at least 90% of the total fluid mass. Data from NIST Webbook [29] for water at 1500 psi and interpolated as a function of temperature was employed in the model. The thermal conductivity of the algae was approximated as 0.1 W/m-K [30], and the thermal conductivity of the mixture λ was calculated as a suspension.

$$\lambda = \frac{\lambda_c\left[\lambda_d + 2\lambda_c - 2P_d\left(\lambda_c - \lambda_d\right)\right]}{\lambda_d + 2\lambda_c + P_d\left(\lambda_c - \lambda_d\right)} \qquad \text{(Eq. 9)}$$

Here, P is the phase volume fraction, λ is the thermal conductivity, and the subscripts c and d mean continuous phase and discontinuous phase, respectively [31].

Water was modeled as a solvent reaction and therefore COMSOL treated the mixture density as the density of the solvent (water). As stated in the two-phase flow section, the density of algae was measured in the Old Dominion Biomass Laboratory as an average of six different samples which was ultimately recorded as 1437.5 kg/m^3 and is in the same range as data found in literature [32]. The density of the products was the mass averaged value of the water and algae. The molecular weight of the algae was taken as 22.3 g/mol, soluble peptides as 22.8 g/mol, and arginine as 174.2 g/mol; these values were calculated from the overall reaction Equation (1) and verified through various websites and literature [33]. All online source material was cross referenced when possible.

2.5 Mathematical Model

Each of the physical processes described previously are governed by conservation laws associated with different mathematical equations. The fluid flow is governed by the Navier-Stokes and continuity equations.

$$\rho(u\cdot\nabla)u = \nabla\cdot\left[-p\mathrm{I}+\mu(\nabla u+(\nabla u)^{T})-\frac{2}{3}\mu(\nabla\cdot u)\mathrm{I}\right] \qquad \text{(Eq. 10)}$$
$$\nabla\cdot(\rho u) = 0$$

In these equations ρ is the density of the material, u is the velocity field, p is the pressure, I is the identity tensor, μ is the dynamic viscosity, and superscript, T, is the transpose operator.

Heat transfer is governed by the conservation of energy and Fourier's Law for steady flow.

$$\rho C_p u\cdot\nabla T + \nabla\cdot q = Q \qquad \text{(Eq. 11)}$$
$$q = -\lambda\nabla T$$

Here, ρ is the density, C_p is the specific heat at constant pressure, u is the velocity field, T is the temperature, Q is the heat source or sink, q is the heat flux and λ is the thermal conductivity.

The magnetic field is governed by the magnetic field equations.

$$\left(j\omega\sigma-\omega^{2}\varepsilon_{0}\varepsilon_{r}\right)\vec{A}+\nabla\times H = J_{e} \qquad \text{(Eq. 12)}$$
$$B = \nabla\times\vec{A}$$

In the magnetic field equations, j is the square root of -1, ω is the radial frequency, σ is the electrical conductivity, ε_0 is the permittivity of free space, ε_r is the relative permittivity, A is the magnetic vector potential, H is the magnetic field intensity, J_e is the external current density, and B is the magnetic flux density.

The transport of the diluted species uses the following equations.

$$\nabla \cdot \left(-D_i \nabla c_i \right) + u \cdot \nabla c_i = R_i$$
$$N_i = -D_i \nabla c_i + u c_i \qquad \text{(Eq. 13)}$$

In this case, D_i is the diffusion coefficient for a given species, c_i is the concentration of species i, u is the velocity field, R_i is the reaction production rate of that species, and N_i is the inward flux of species i.

2.6 Numerical Model

2.6.1 Reactor Model Geometry

The COMSOL model is assumed to be axisymmetric, which reduces solution time greatly. This means that the coils are modeled as closed loops instead of one helix shape. The basic geometry of the reactor in the mobile pilot unit is shown schematically in Figure 5.

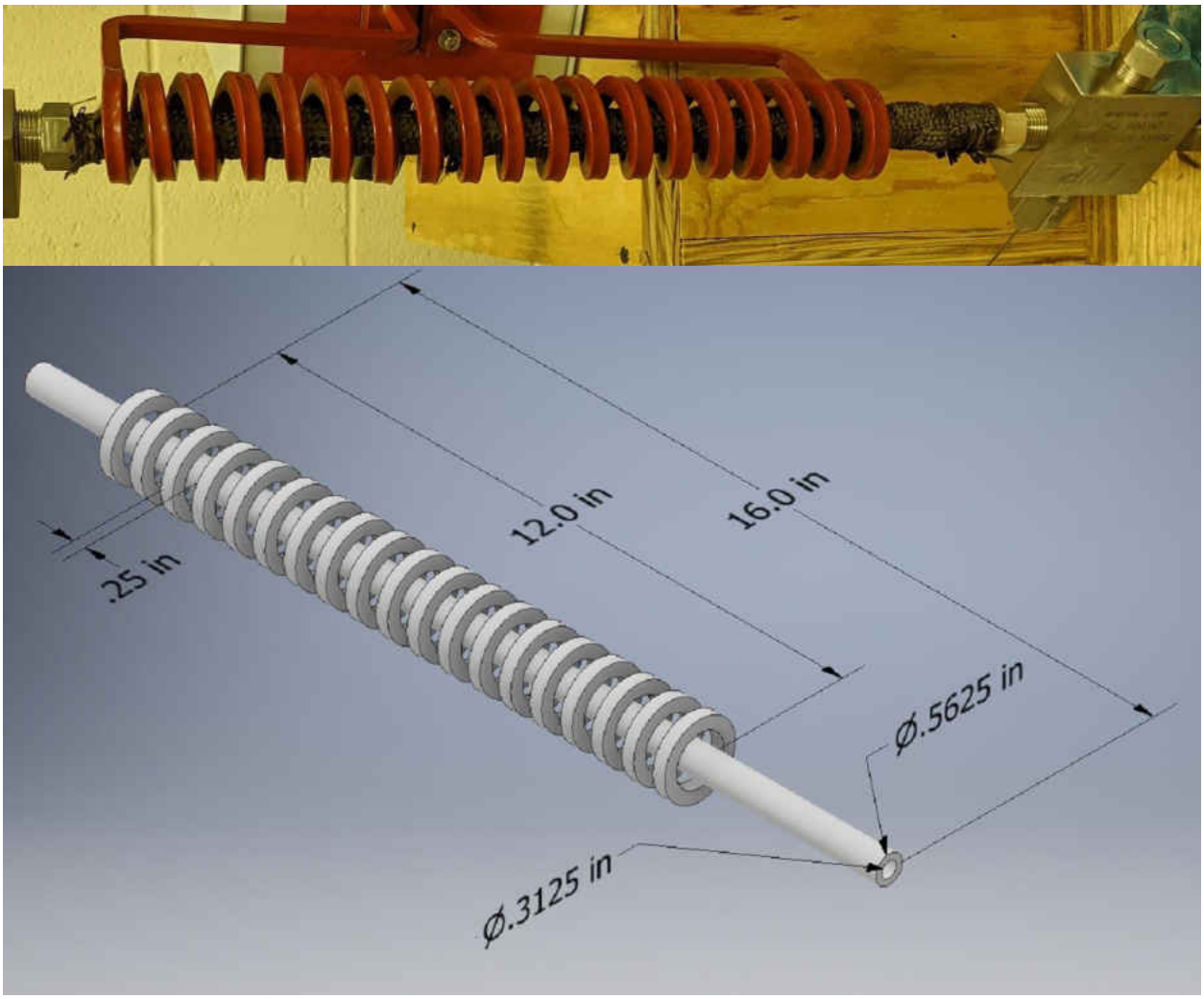

Figure 5. Geometry of the mobile pilot unit reactor. Actual reactor (top) and a 3D model with axisymmetric assumption (bottom).

Included in the model are infinite domain elements in the air domain which are often used in magnetic field models and they treat the small layer they are assigned to as a much larger area so that meshing can stay reasonable but the coils are far away from any magnetic insulation boundaries. The reacting flow domain has a radius of $^{5}/_{32}$ inches (4 mm). The pipe is ⅛ inches

(3.2 mm) in thickness. The coils are $^1/_4$ inches (6.35 mm) square and have $^1/_8$ inch square water passages located concentrically inside.

2.6.2 Physical Boundary Conditions

After defining the reactor geometry and specifying associated materials, the five coupled physical phenomena occurring in the reactor were modeled. They are convective and radiative heat transfer, laminar fluid flow, magnetic field effects (with their associated electrical currents), transport of dilute species (algae), and the associated chemical reactions. Modeling the physics required the development of a set of coupled differential equations. The associated boundary conditions have been defined in the subsections that follow. Axial symmetry with respect to the flow axis was assumed for all aspects of the model.

2.6.2.1 Heat Transfer Boundary Conditions

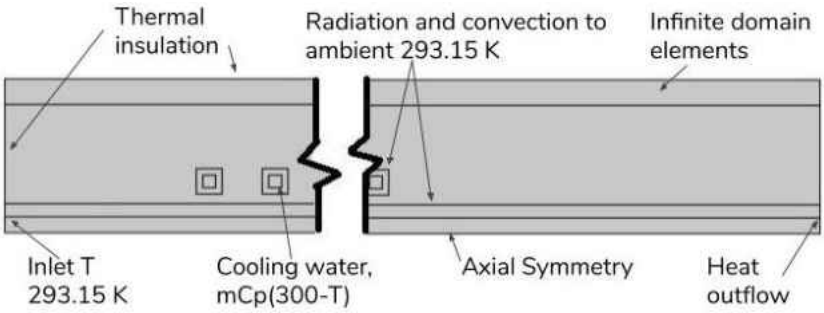

Figure 6. Heat transfer boundary conditions

The heat transfer boundary conditions are as follows: a uniform inlet flow temperature of 293.15 K, a heat outflow (open boundary), a cooling water heat sink within the coils based on a specified flow rate and specific heat based thermal capacity, net radiation and convection heat transfer balances on the boundaries (interacting with surrounding atmosphere), and thermal

insulation along the outer edges of the modeling domain. These insulated boundaries are far away from the heat source with the help of the infinite domain elements that have been discussed in the reactor model geometry. The cooling water mass flow rate was 8 kg/s, a value specified by the chiller manufacturer, and the average cooling water temperature was (300 K), as indicated by the chiller temperature display during normal test operating conditions.

2.6.2.2 Laminar Flow Boundary Conditions

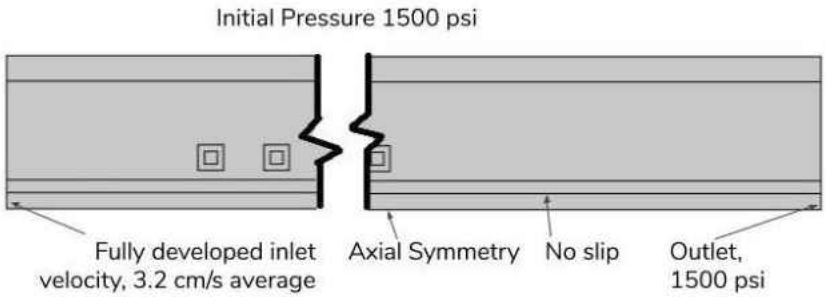

Figure 7. Laminar flow boundary conditions

The pipe flow was assumed to be a fully developed axisymmetric laminar profile. The flow velocity was specified with the velocity profile, Equation (4), which yields a mean velocity of 3.2 cm/s. A uniform pressure outlet condition of 1500 psi was specified and a no slip boundary condition is placed on the inner pipe surface.

2.6.2.3 Magnetic Field Boundary Conditions

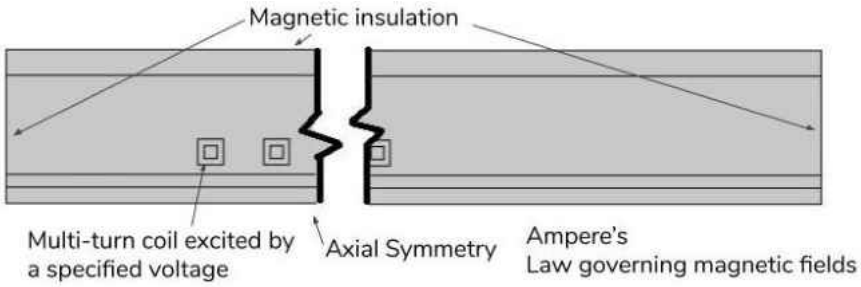

Figure 8. Magnetic field boundary conditions

A COMSOL multi-turn coil function was employed for the copper coils which excites them with a specified voltage and subsequently generates a magnetic field around them. A magnetic insulation condition was imposed along the outer edge of the entire geometry. Ampere's Law represents the magnetic fields in the geometry and there are no further boundary conditions needed because the coil feature inherently includes all the necessary coil excitation information.

2.6.2.4 Transport of Diluted Species Boundary Conditions

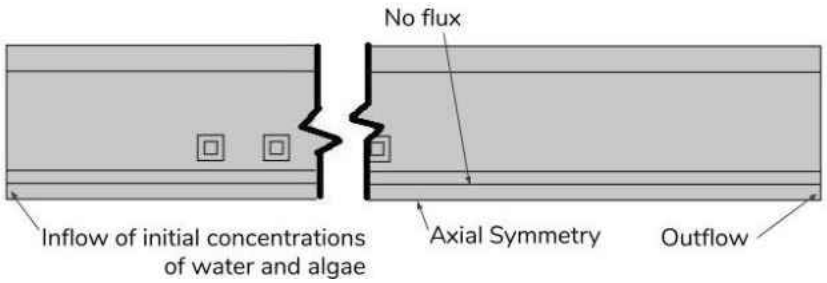

Figure 9. Transport of diluted species boundary conditions

The flow enters the reactor with specified initial concentrations of the reactants and water, assuming 10% algae to water mixture by mass. The 10% algae component was assumed

to be 54% protein and 16% of that protein was assumed to be arginine. A no flux condition (impermeable boundary) was applied to the pipe wall. The outflow (open boundary) was specified at the exit of the flow from the reactor

2.6.3 Model Solution Mesh

In order to minimize numerical error, the finest mesh possible (limited by computational resources) was selected for all the numerical studies. Triangular elements meshed most of the domain and smaller boundary layer elements were introduced on the pipe wall surface. The triangular elements were smaller when they were in close proximity to the boundary elements for a smooth size transition. The finer boundary elements are important for more accurate calculation of the fluid velocity profile and the heat transfer near the pipe wall. Smaller triangular elements were specified around the coils for accurate calculation of the magnetic field influences. Infinite domain elements were used primarily to manage the field equation computational resources requirements while keeping the coils away from the magnetic insulation boundaries. An example of the mesh elements is shown in Figure 10. This mesh is intentionally very coarse so the types of elements can be seen easily.

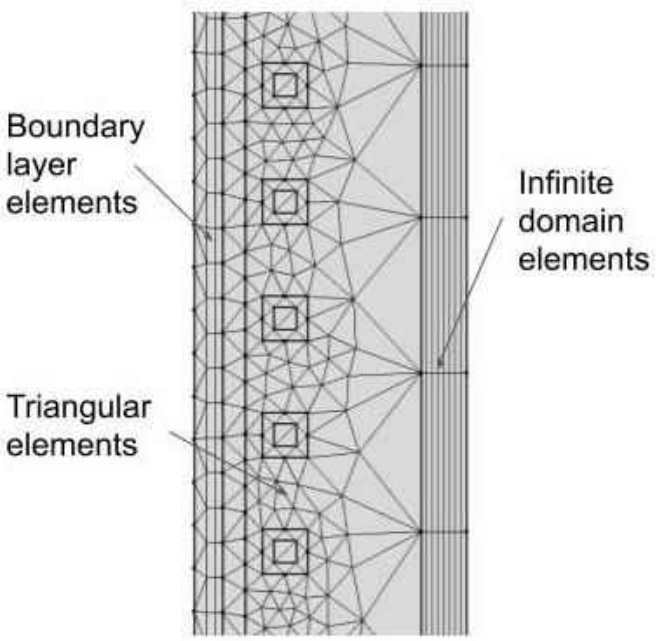

Figure 10. Typical coarse mesh of a portion of the domain

2.7 Non-COMSOL Calculations

2.7.1 Reactor Residence Time

Residence time, which is the time that the algae and water slurry spends in the reactor, is important because product yields vary with the reaction time. Accounting for velocity influences, residence time changes with the density ratio as:

$$t = \frac{V}{F \cdot \left(\frac{\rho_{pump}}{\rho_{T,P}} \right)} \qquad \text{(Eq. 14)}$$

In this equation, V is reactor volume, F is the volumetric flow rate, ρ_{pump} is the density of the flow after pump pressurization but before heating, and $\rho_{T,P}$ is the density of the flow at the

intended reaction temperature. The reactor length is 16 inches (0.406 m), which is the distance from the start of the heating coil to the exit thermocouple. The residence time formula can be used in two ways: to fix the residence time and calculate the flow rate, or to calculate the residence time from a given flow rate.

2.7.2 Effective Composite Heat Transfer Coefficient

There are two modes of heat transfer away from the reactor: natural convection to the ambient and radiation to the surroundings. Radiation is controlled in COMSOL by material emissivity and convection is included with a specified heat transfer coefficient. The convection is specified and not simulated with airflow fluid dynamics to avoid severe computational resource demands that would be imposed by a quasi-periodic coil winding and gap configuration exchanging energy with itself and the surroundings. Radiant thermal exchange was calculated with view factors which are verified in a later section. However, there is also a thin insulation layer surrounding the reactor, which is not modeled in the COMSOL geometry, so its thermal effect needs to be modeled together with the uninsulated convection coefficient in an overall composite heat transfer coefficient. The thermal resistance heat transfer method was utilized to consider both the conduction through the concentric cylinders (pipe surface and outer surface of the insulation) and the natural convection together. The simplified thermal resistance model to determine an overall composite heat transfer coefficient was

$$\frac{1}{h_{total}} = \frac{d_{outside} \cdot \ln\left(\frac{d_{outside}}{d_{inside}}\right)}{2\lambda} + \frac{1}{h_{convection}} \qquad \text{(Eq. 15)}$$

In this equation, the diameter of the reactor with and without the insulation wrap ($d_{outside}$ and d_{inside}) were utilized along with the thermal conductivity (λ) to estimate conduction resistance. The convective heat transfer coefficient ($h_{convection}$) was estimated utilizing a correlation explained later in this section. Pipe conduction is modeled directly by COMSOL as part of the defined geometry, and the conduction through the insulation was minimal; the thermal conductivity for a fiberglass exhaust wrap was approximately 0.28 W/m-K for thin blanket fiberglass fabrics and the thickness of the wrap was $^1/_{16}$ inches [28]. Nusselt number ($Nu = h*D/\lambda$) was correlated with a Rayleigh number (Ra) based on the ratio of the height of the cylinder to the diameter and is valid for this case [34].

$$Nu = A*Ra^n \quad \text{where,}$$
$$A = 0.519 + 0.03451(L/D) + 0.0008772(L/D)^2 + 8.8555 * 10^{-6}(L/D)^3 \qquad \text{(Eq. 16)}$$
$$n = 0.25 - 0.00253(L/D) + 1.152 * 10^{-5}(L/D)^2$$

Here, L is the length of the reactor and D is the outside diameter of the reactor. After the Nusselt number was calculated, the heat transfer coefficient was determined employing the thermal conductivity of the surrounding air, λ. All air properties were evaluated at a mean temperature of the surface and surrounding air. This calculation was used iteratively for all versions of the model because it is codependent on the surface temperature. Therefore, the surface temperature was evaluated after every model solution to verify that the correct heat transfer coefficient estimate was utilized.

2.8 Model Validation

2.8.1 Experimental Validation

2.8.1.1 Mass and Energy Balances

A fundamental check of model quality was verification of mass and energy balances based on the fundamental laws of conservation of energy and conservation of mass. Overall balances were computed after every modeling change. Mass flow rates verification utilized integration of varying local density multiplied by the associated velocity across an axial cross section. Balance is achieved when the inlet and outlet mass flow rates equate. The computed values were also checked manually employing the density of the algae and water slurry, the average inlet velocity, and the cross-sectional area of the tube.

Energy balances can be validated in several ways, the first of which is to compare the heat sources and sinks in the reactor model domain (including sources from induction heating and defined sinks to the surroundings and energy removed by the cooling water) to the energy flow rate leaving the model domain [35]. This method is the simplest to implement in COMSOL. It was also possible to balance the electromagnetic heating of the pipe with the heat added to the flow plus the heat dissipated from the pipe surface. The convected energy equation $Q = \bar{m} * C * T$ was used to calculate the thermal energy change between the reactor inlet and outlet. Those balances produced errors of less than one percent, which was considered to be consistent with the accuracy of the model.

2.8.1.2 Surface-to-Surface Radiation

COMSOL utilizes a surface-to-surface radiosity model to determine view factors and the resultant radiation heat transfer. When implemented, the computed radiosity for each surface was

employed to determine the surface temperature-based radiation heat transfer. In order to validate the COMSOL implementation of the model, a spreadsheet was created using basic view factor tabulation and radiosity estimates based on a simplified geometry. The simplified geometry was a length of reactor equal to the center-to-center distance between coils and an adjacent coil surface. Nominal pipe surface and coil temperatures were assumed, along with the ambient temperature, in estimating the radiosities and resulting pipe surface radiation loss. By considering eight different coil sections along the entire length of the coil, summarized in Table 2, the individual coil based radiosity approximations produced radiation cooling estimates within 3% of the COMSOL radiosity calculations.

Table 2. Radiosity verification checks

Pipe Surface Temperature (K)	Coil-based Radiosity (W/m^2)	COMSOL Radiosity (W/m^2)	% Difference
436	1510	1550	2.58
686	6580	6700	1.79
791	11500	11650	1.29
864	16300	16500	1.21
893	18500	18825	1.73
915	20400	20725	1.57
916	20500	20850	1.68
889	18200	18350	0.82

2.8.1.3 Comparison with Experimental Results

Experiments were conducted employing water without any algae as the test fluid for three different flow rates and controlled output temperatures. The purpose of the experiments was to collect induction heating operating conditions for input into COMSOL for comparison, but the axisymmetric assumption prevented the modeling of a rectangular manifold block with a thermocouple. A three-dimensional COMSOL manifold block geometry was created to permit better interpretation of the measured thermocouple temperatures. Water velocity and temperature profiles exploiting axial symmetry were imported to create temperature and velocity profiles at the inlet to the manifold block. Figure 11 shows the model of the manifold block and the thermocouple within:

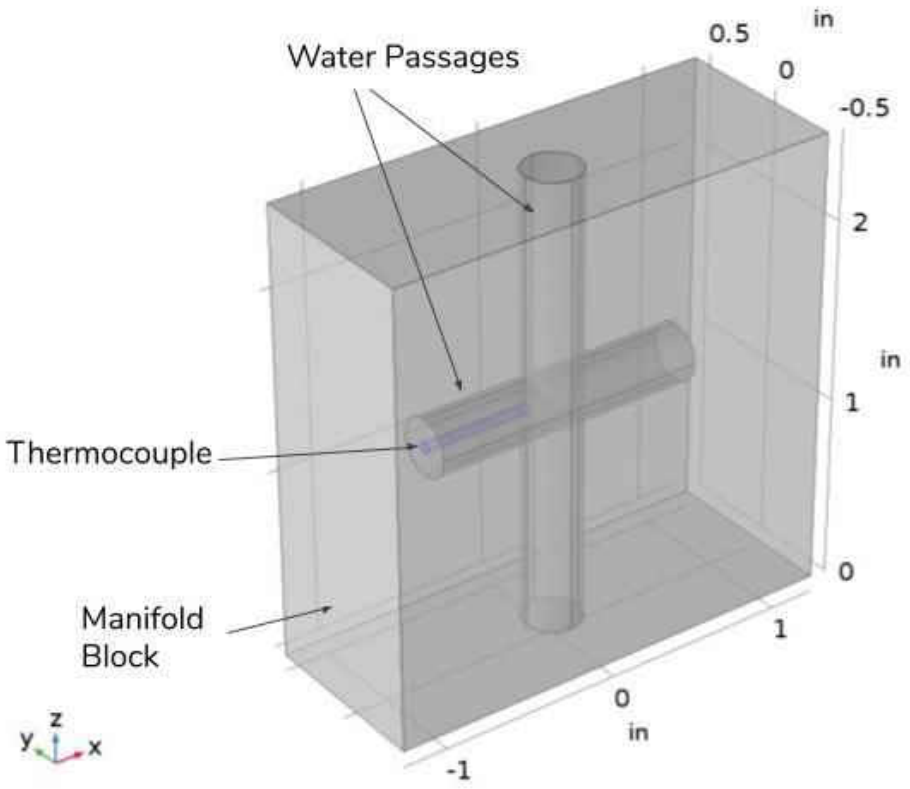

Figure 11. COMSOL manifold 3D model

The manifold was fabricated from 316 stainless steel with a through hole from the top to the bottom. The thermocouple was modeled as a cylinder of diameter $^{1}/_{16}$ inches (1.6 mm) and extends slightly into the flow. The average thermal conductivity of the thermocouple at the model temperature is 17.5 W/m-K. Radiation and convection losses to the surrounding atmosphere due to the exterior surfaces of the manifold were calculated. Employing this model produced an accurate estimation of the relationship between the thermocouple and (water) feedstock temperature. The five experimental test conditions are summarized in Table 3.

Table 3. Validation experimental data

Experimental (Thermocouple) Temp. (^{o}C)	Flow Rate (mL/min)	Coil Power (W)	Current (A)	Voltage (V)	COMSOL (Thermocouple) Temp. (^{o}C)	Percent Difference
150	81	1500	70	180	154.0	2.7
300	118	4500	100	323	316.0	5.3
150	118	2000	77	210	159.9	6.6
300	81	3500	92	280	306.6	2.2
280	95	3350	91	275	277.8	0.8

Percent differences of less than seven percent were considered acceptable for the purposes of this modeling. Model consistency is quite good for the desired outlet temperature of 280 ^{o}C and a flow rate of 95 mL/min.

2.8.1.4 Coil Electrical Conductivity

Coil electrical conductivity (the inverse of resistivity) is based on the overall coil resistance, length, and cross-sectional area. The coil electrical conductivity was chosen so that

the model resultant temperatures would match experimental results to adjust for uncertainty in the coil length and resistance. That analysis resulted in an estimated value of 1.35 x 10^5 S/m which produced model flow temperatures in agreement with experimental results. To verify the validity of this result, a three-dimensional model of the coil was created employing *Autodesk Inventor* to estimate the actual length of the coil. On that basis, the coil length was 2.00 meters. Consequently, the coil resistivity was:

$$\rho_e = \frac{R \cdot A_c}{L_c} \qquad \text{(Eq. 17)}$$

where R is resistance, A_c is the cross-sectional area of the copper coil excluding the water-cooled core, and L_c is coil length. As for the resistance of the coil, Equation 7 (where power in the coil is related to resistance and current) was employed. The measured current and power were recorded during some validation experiments (Table 3). The average measured coil resistance was 1.73 x 10^5 S/m (28% higher than the estimate). Since actual material resistance depends on copper purity and dimensional precision, the value that matched experimental results (1.35 x 10^5 S/m) was satisfactory.

2.8.2 Mesh Refinement Analysis

A mesh refinement analysis is an important aspect of any CFD or FEA study. Mesh refinement helps to establish confidence in the results while assessing the numerical accuracy based on finer mesh geometries. The basic procedure for a mesh refinement analysis is to perform simulations with increasingly finer solution resolutions to compare overall variations in

terms of computational overhead. Nine mesh resolutions were utilized in the study and were assigned a number nominally in order of increasing resolution. Mesh element statistics of the nine resolutions are as follows:

Table 4. Mesh element statistics

Mesh Number	Number of Triangular Elements	Number of Quadrilateral Elements	Average Element Quality
1 (Extremely Coarse)	1647	346	0.7022
2 (Extra Coarse)	2122	460	0.7069
3 (Coarser)	2828	618	0.7403
4 (Coarse)	4582	850	0.7686
5 (Normal)	6691	1098	0.8226
6 (Fine)	9229	1282	0.8395
7 (Finer)	27258	2384	0.898
8 (Extra Fine)	82868	4306	0.9283
9 (Extremely Fine)	100182	4698	0.9415

The influence of grid resolution on temperature and velocity of the reacting flow were chosen for the refinement study. Since these model outputs cannot be compared to other simulations or experimental results, the mesh resolution influences were isolated by comparison with the finest mesh resolution (mesh 9). The root mean square differences as compared with the finest mesh measures mesh sensitivity. Root mean square differences that decrease as the mesh density is increased is a persuasive argument supporting the model accuracy. Temperature and velocity were evaluated at 240 equally spaced points plotted along two axial lines in the reactor:

the centerline, T(0, z) and two thirds of the distance from the centerline to the pipe wall, T(R/2.65 mm, z), (referred to subsequently as "near wall"). All 480 points were included in the root mean square calculation for temperature and velocity. Shown below are temperature and velocity at the centerline for the mesh resolutions:

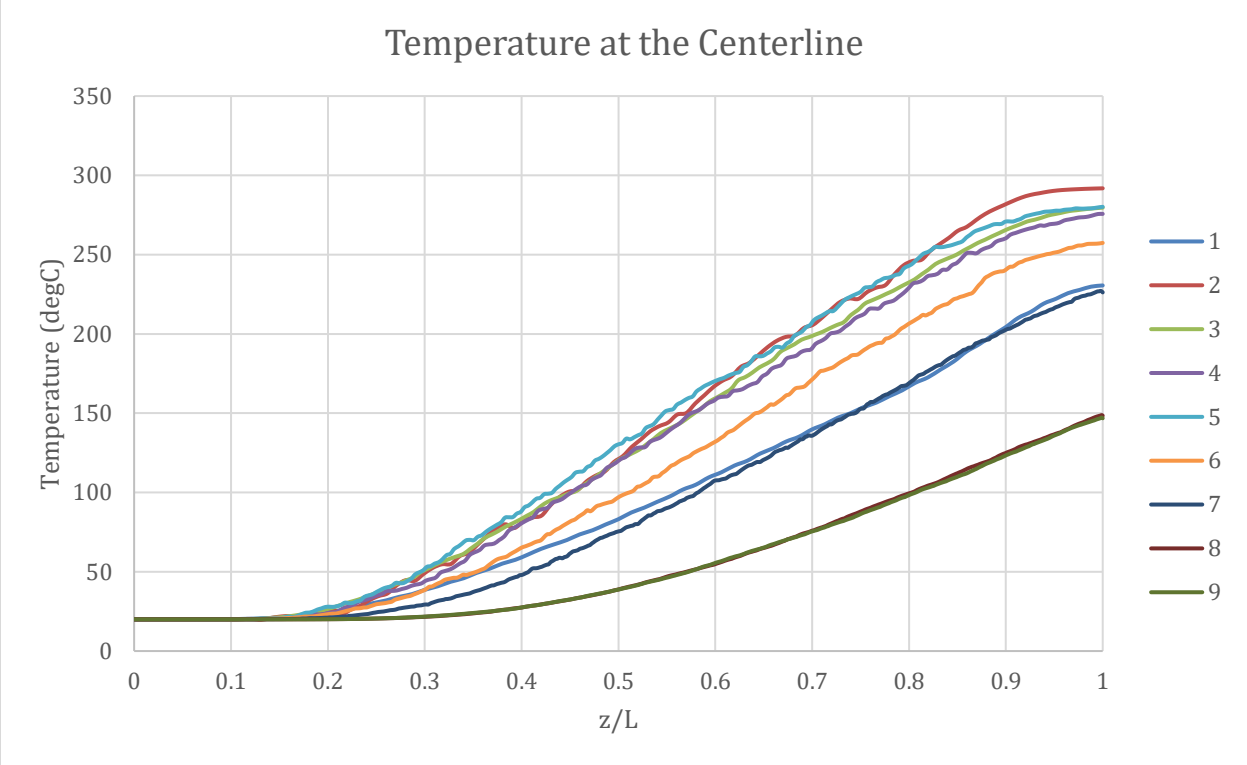

Figure 12. T(0, z/L) of the mesh resolutions

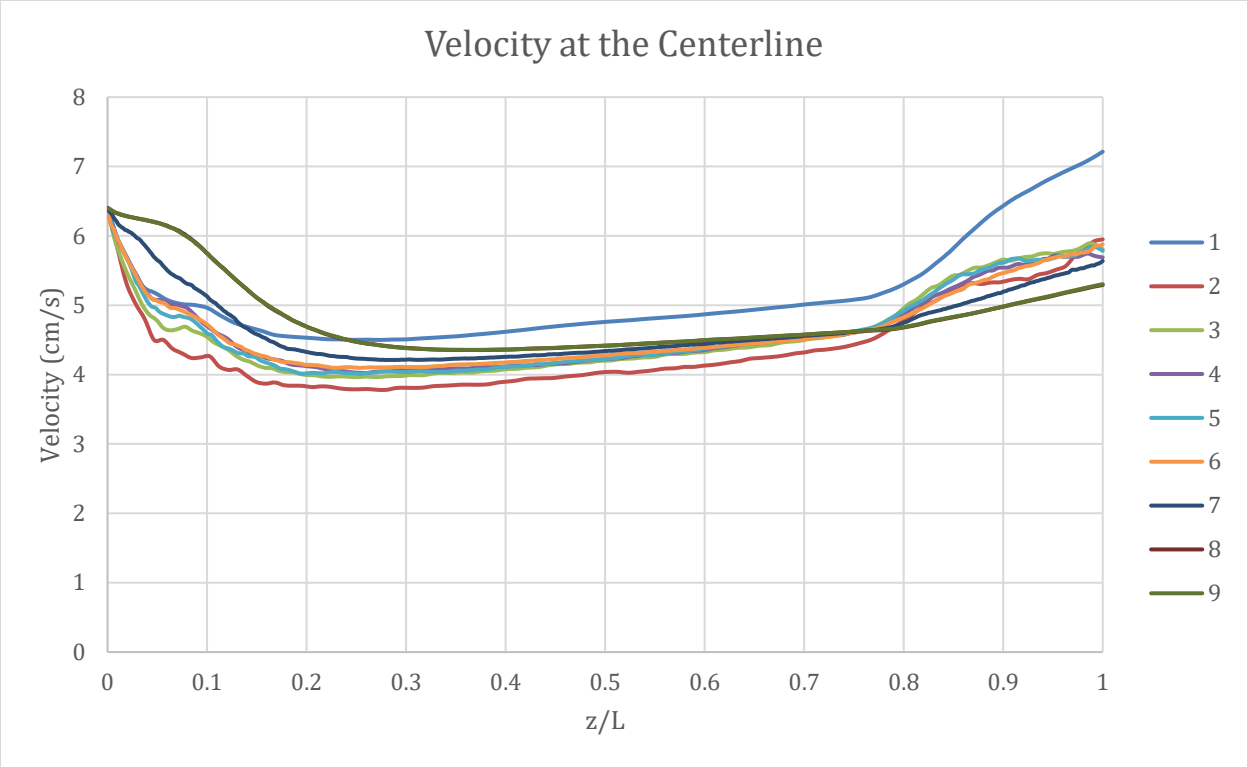

Figure 13. V(0, *z/L*) of the mesh resolutions

Mesh resolution improvements are shown as the plotted temperatures and velocities converge toward the highest mesh number. The root mean square differences are computed between the points on the mesh 1 and mesh 9 curves for both the centerline and the near wall line (graphs in Appendix A) and included together for mesh refinement analysis:

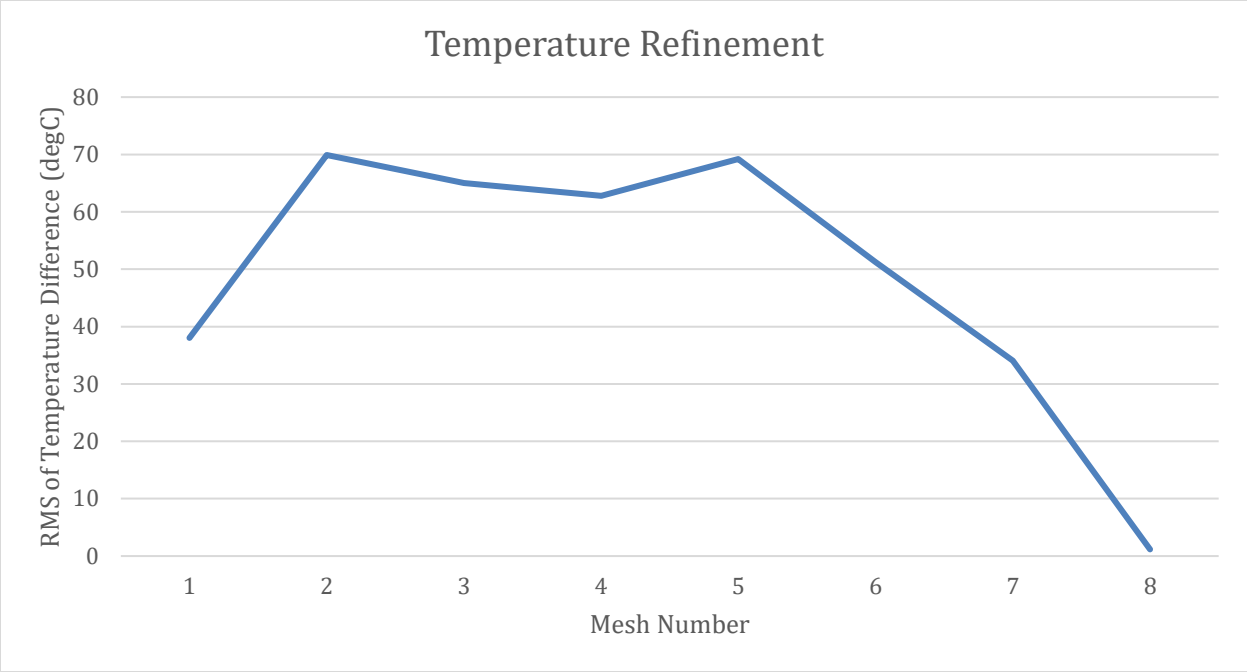

Figure 14. Root mean square of the temperature difference between progressively finer meshes and the finest mesh

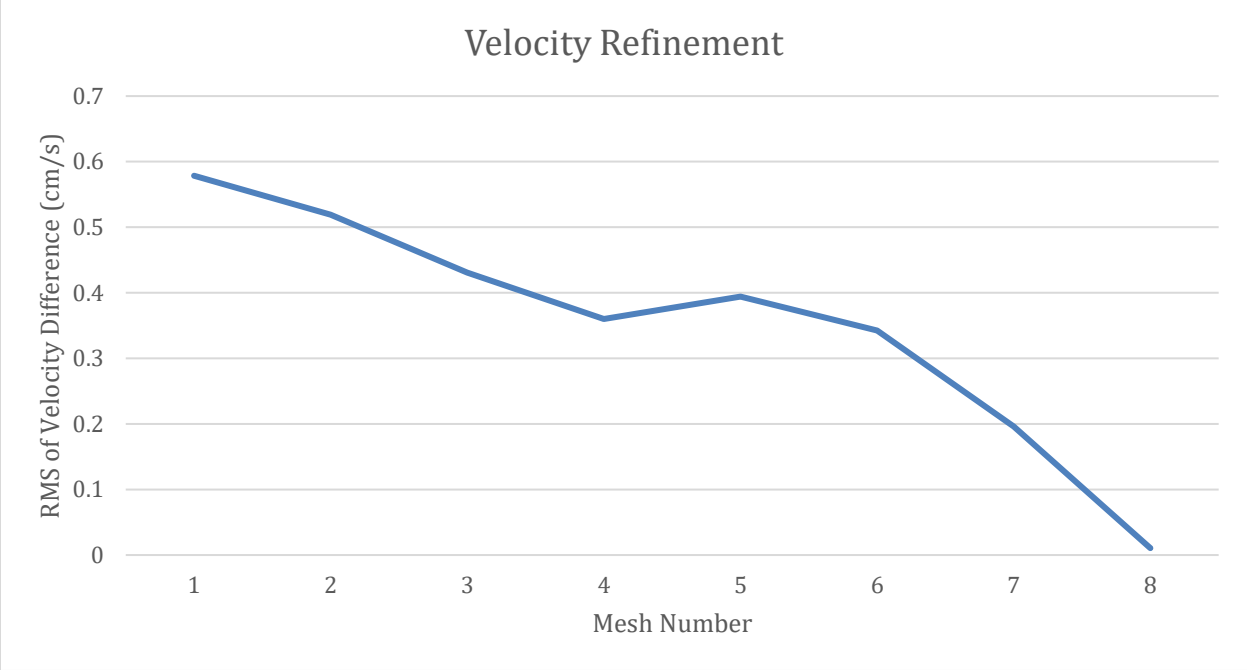

Figure 15. Root mean square of the velocity difference between progressively finer meshes and the finest mesh

The mass flow rates and the energy balances were also plotted as the mesh resolution increased. The calculation procedure has already been explained in the mass and energy balances section.

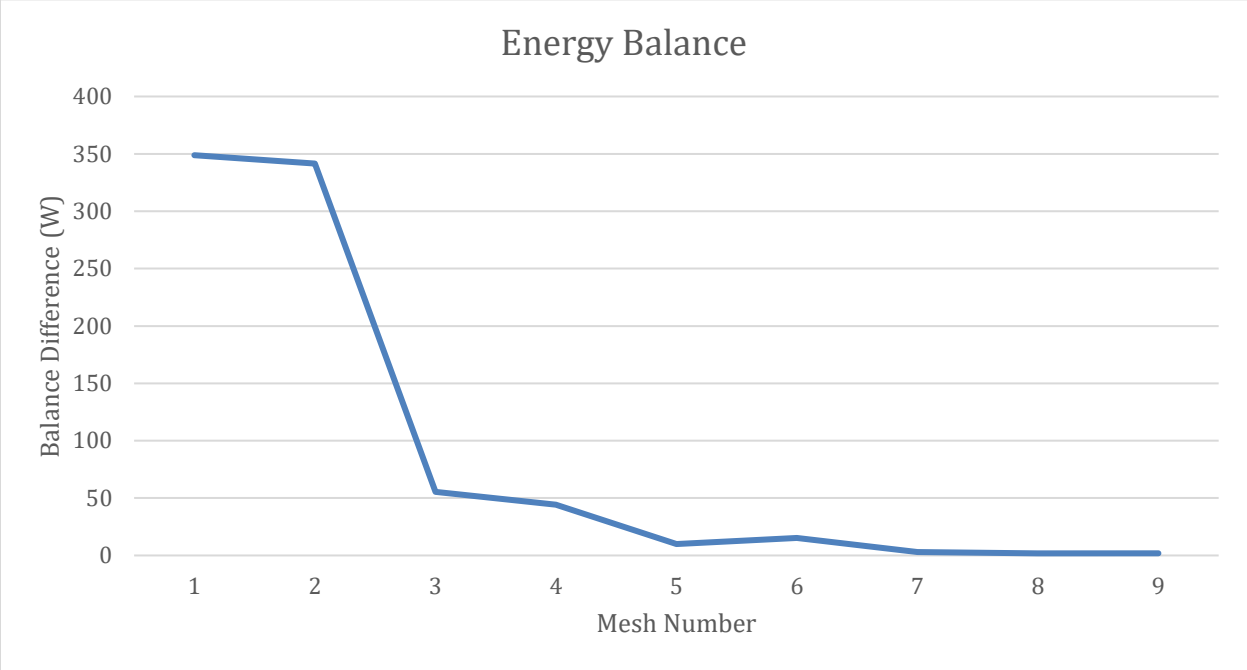

Figure 16. Difference between heat generated in the model and thermal energy leaving the model

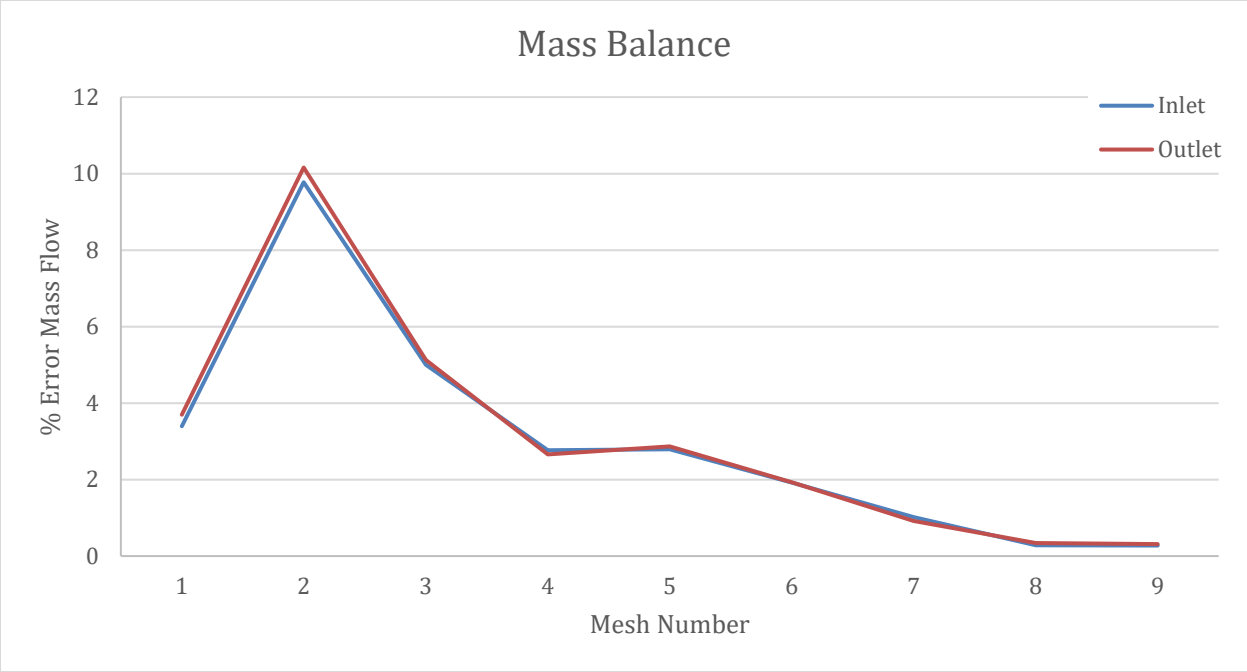

Figure 17. Percent difference between inlet and outlet mass flow rates and the analytical

All of the presented results are consistent with what is expected. The mass and energy balances show improved convergence with increasing mesh resolution. On that basis the finest mesh resolution appears to produce acceptable accuracy. As mentioned previously, the mass balance and energy balances are within one percent when evaluated at the finest mesh. More plots of temperature, velocity, and conversion of algae can be found in Appendix A.

CHAPTER 3

RESULTS

3.1 Baseline Case

The design intent of the mobile pilot unit reactor is to achieve controlled conversion reactions with a ten percent mass concentration algae slurry feedstock. The baseline design flow rate is 95 mL/min, based on a thermocouple-controlled output temperature of 280 ºC. Results of these simulations are shown in Figures 18-20:

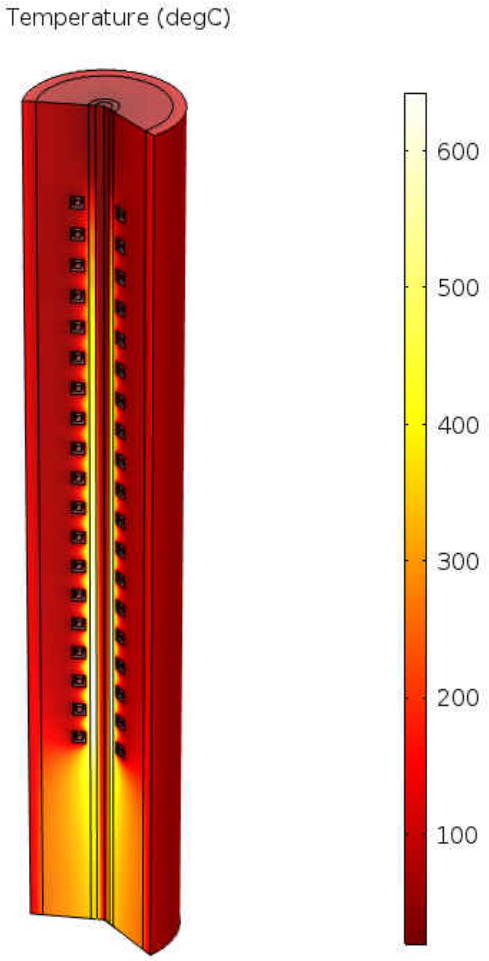

Figure 18. Temperature variation throughout model for baseline conditions

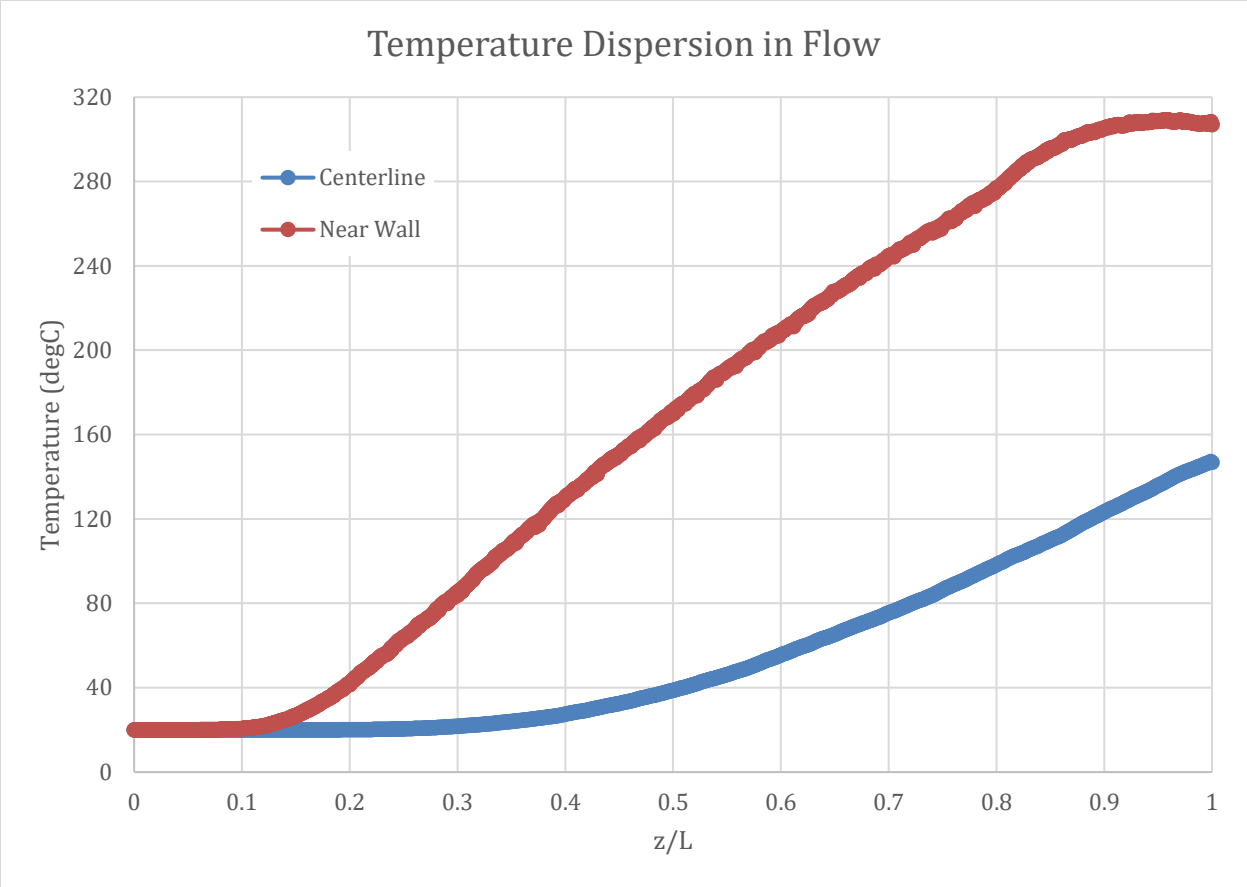

Figure 19. Variation of centerline T(0, *z*) and T(*R*/2.65 mm, z) along the reactor

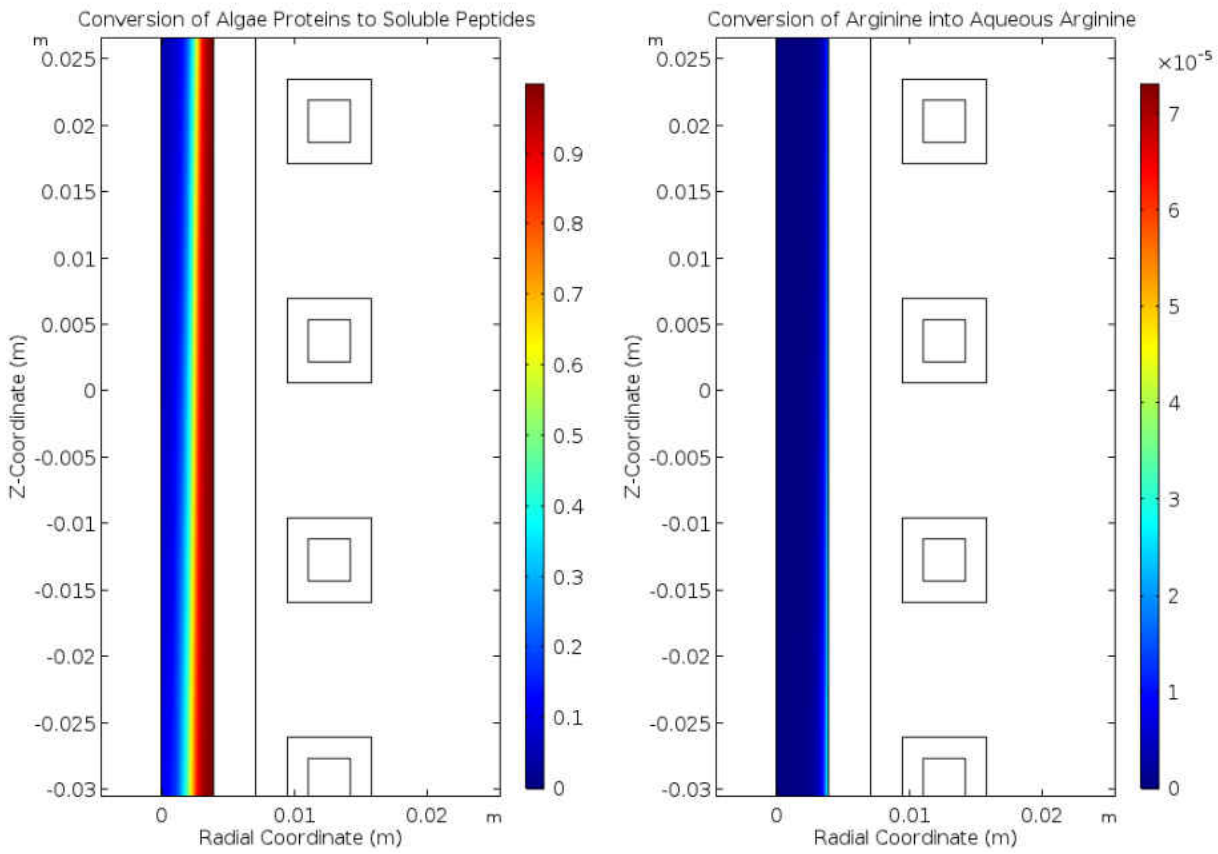

Figure 20. Protein (left) and arginine (right) conversion (reactants converted between 0 and 1) for the baseline case in a center portion of the reactor.

The predicted temperature distribution was expected since some areas of the pipe were heated above 600 ºC due to the induction heating skin effect. Furthermore, there is a large difference between the centerline fluid temperature and the near wall temperature. The simulated thermocouple temperature at the manifold location was 277.8 ºC. Conversion (between 0 and 1) measures the amount of reactant converted to product and is based on concentrations, with $x_i = (c_{i0}-c_i)/c_{i0}$. The algae was initially composed of 54% proteins in a solid state (Figure 1). At the reactor outlet, the model predicts 6.2% of proteins have not been solubilized. In terms of mass, 50.8 g of proteins have been converted to soluble peptides per 100 g of algae. The arginine

conversion was not nearly as successful; the conversion to aqueous arginine is only 1.7×10^{-5} leaving the reactor. This is likely due to the much lower forward frequency factor (response time rate) of the arginine reaction compared to the protein.

3.2 Design Sensitivity Analysis

One of the goals of this research was to identify key design parameters with the greatest potential to enhance mobile pilot unit performance. With that in mind, design parameters were chosen for study in a sensitivity analysis. The reactor performance was evaluated in terms of maximum centerline conversion of proteins to soluble peptides, ratio of concentration of proteins to soluble peptides at the reactor outlet, average outlet temperature, and axial reactor location for 97% conversion of algae proteins near the wall. For each parameter, higher and lower values than the baseline case values were chosen one at a time. All other variables were held constant as much as possible. Some design variable inconsistencies were unavoidable; a change in the outer-pipe diameter altered the coil diameter because the gap between the coil and the outer surface of the reactor was to be held constant. The reaction residence time was kept constant when changing the reactor diameter by altering the slurry mass flow rate. Each high and low value required a new model utilizing the finest resolution mesh available. Table 5 summarizes the sensitivity values:

Table 5. Design characteristic parameters for sensitivity analysis

	High Value	Standard	Low Value
Coil Pitch (turns/in)	2.3	1.6	1.2
Coil Frequency (kHz)	320	285	250
Reactor Pipe Diameter (in)	7/16	5/16	3/16
Residence Time (s)	15	10	5
Algae Concentration (% by mass)	15	10	5
Pipe Wall Thickness (in)	3/16	1/8	1/16
Pipe Emissivity	0.9	0.5	0.1

The results of the sensitivity analysis are tabulated below as percent differences from the standard model values. The high value and low value columns correspond to the high and low values of the design characteristic in Table 5.

Table 6. Centerline protein conversion sensitivity

Baseline Centerline Protein Conversion		0.834
	High Value	Low Value
Coil Pitch	8%	-14%
Excitation Frequency	-5%	5%
Pipe Diameter	-80%	20%
Residence Time	18%	-65%
Algae Concentration	6%	-13%
Pipe Wall Thickness	-4%	15%
Pipe Emissivity	-2%	2%

Table 7. Ratio of proteins to soluble peptides (products to reactants) at the reactor outlet sensitivity

Baseline Ratio of Proteins to Peptides at the Reactor Outlet		0.124
	High Value	Low Value
Coil Pitch	-36%	76%
Excitation Frequency	31%	-26%
Pipe Diameter	926%	-100%
Residence Time	-91%	728%
Algae Concentration	-29%	73%
Pipe Wall Thickness	23%	-68%
Pipe Emissivity	9%	-10%

Table 8. Average outlet temperature sensitivity

Baseline Outlet Temperature		246.6 (^{o}C)
	High Value	Low Value
Coil Pitch	-3%	-2%
Excitation Frequency	-9%	10%
Pipe Diameter	-46%	146%
Residence Time	39%	-40%
Algae Concentration	0%	0%
Pipe Wall Thickness	-8%	12%
Pipe Emissivity	-4%	6%

Table 9. Axial location near wall where 97% conversion of proteins to soluble peptides sensitivity

Baseline 97% Near Wall Protein Conversion Axial Location		0.356 (m)
	High Value	Low Value
Coil Pitch	-15%	16%
Excitation Frequency	6%	-7%
Pipe Diameter	Insufficient Length	-51%
Residence Time	-31%	Insufficient Length
Algae Concentration	-7%	12%
Pipe Wall Thickness	5%	-7%
Pipe Emissivity	3%	-2%

It should be noted that the reaction model does not account for overheating of the algae slurry, which is possible in some cases but currently unquantifiable. As expected, reactor pipe diameter changes had the greatest influence as smaller diameter produced the highest exit temperatures and the larger diameter had heating limitations. With the smaller diameter, the flow rate was decreased to approximately one third of the baseline flow in order to maintain the desired residence time. Residence time was also a strong factor in all of the performance metrics because the slurry had more or less time in the reactor to heat up. Another expected result was thinner pipe wall thicknesses permitted more efficient slurry heating due to less thermal resistance between the skin effect heating zone and the feedstock. Pipe emissivity was not a very significant factor. Of the changes requiring the least hardware modification, residence time via flow rate alteration had the greatest influence on predicted results. However, smaller diameter thin-walled reactor tubes most likely would have the greatest practical impact.

COMSOL calculates the resistance of the coil based on coil electrical conductivity, pitch, and length. Coil pitch changes altered the coil power because the current was assumed to be constant. This led to some counterintuitive results, starting with the larger coil pitch significantly improving all performance metrics. Shown below is the high coil pitch compared to the baseline:

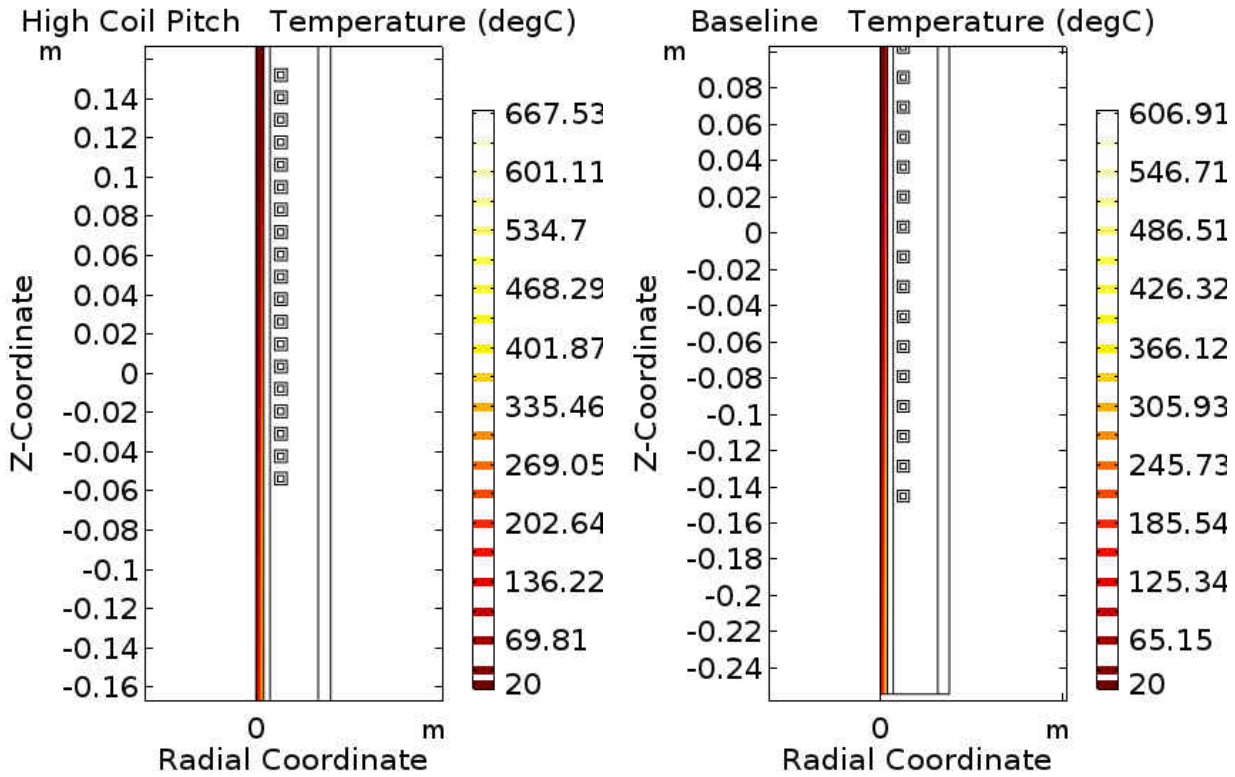

Figure 21. High coil pitch (left) versus baseline (right) on temperature

Interestingly, although the slurry had less direct coil heating time, the feedstock still reached higher maximum local feedstock temperatures than the baseline case. Consequently, the outlet temperature profile became more nearly uniform, so the outlet temperature actually decreased unlike that associated with smaller diameter tube. The temperature variation along the outer

surface of the reactor in the high coil pitch model exhibited higher peak values. However, local cooling by the ambient environment attenuated those peaks along the non-heated remainder of the reactor. The baseline case produced a maximum reactor tube surface temperature approximately 75% down the length of the reactor. At the same reactor axial location, the low high coil pitch model had a cooler surface by approximately 250 ºC.

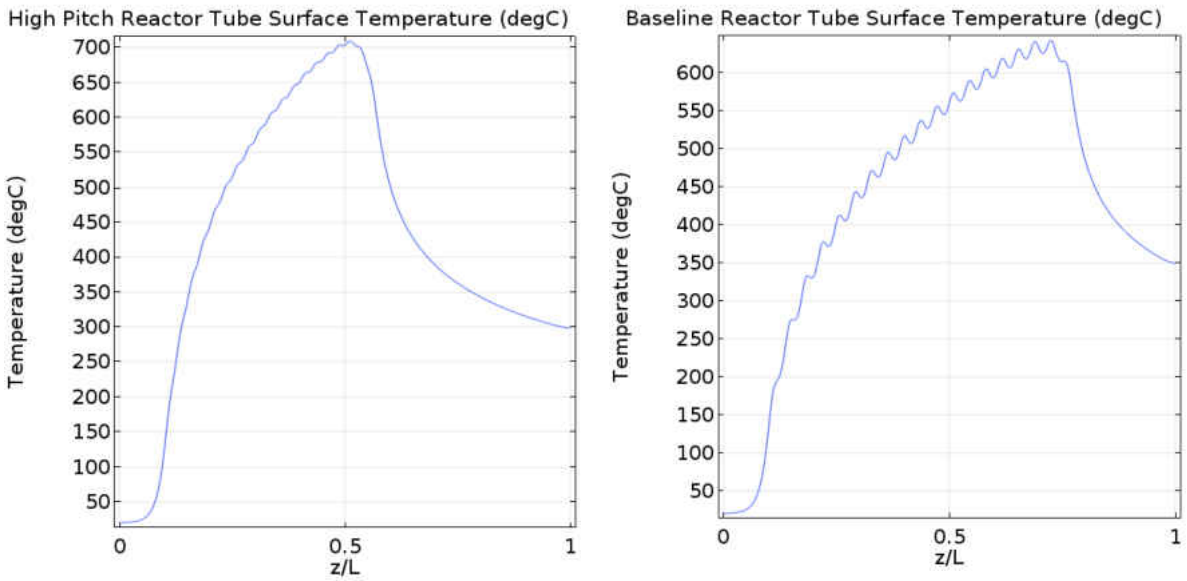

Figure 22. T(*R/* 7.14 mm, *z/L*) for the high coil pitch (left) and baseline (right) models

This a noteworthy finding because it indicates that it may be possible to heat the slurry in a shorter time and allow it to equilibrate more uniformly before cooling while maintaining the desired residence time. This also suggests it may be possible to operate the feedstock stream with a reactor exit temperature below 280 ºC while achieving maximum protein conversion. This should merit further exploration.

Lower induction excitation frequency produced similar results to the high coil pitch simulation other than the temperature at the outlet which was noticeably higher. Although the maximum flow temperature of the low frequency model was almost the same as for the high coil

pitch case (671 ºC vs. 668 ºC), the average predicted temperature at the outlet was 30 ºC higher in the former. Lower frequency means skin effect heating penetrates deeper into the reactor tube while requiring more power [16]. Thus, a lower frequency heated more of the pipe thickness and conducted the heat to the slurry with reduced conduction resistance.

Finally, the simulations showed that increasing algae concentration improved all of the relevant quality metrics. All of the flow thermodynamic properties were calculated based on the concentration and are accurate approximations. Below is the conversion of proteins in the high concentration model compared to the baseline case at both the centerline and near the wall:

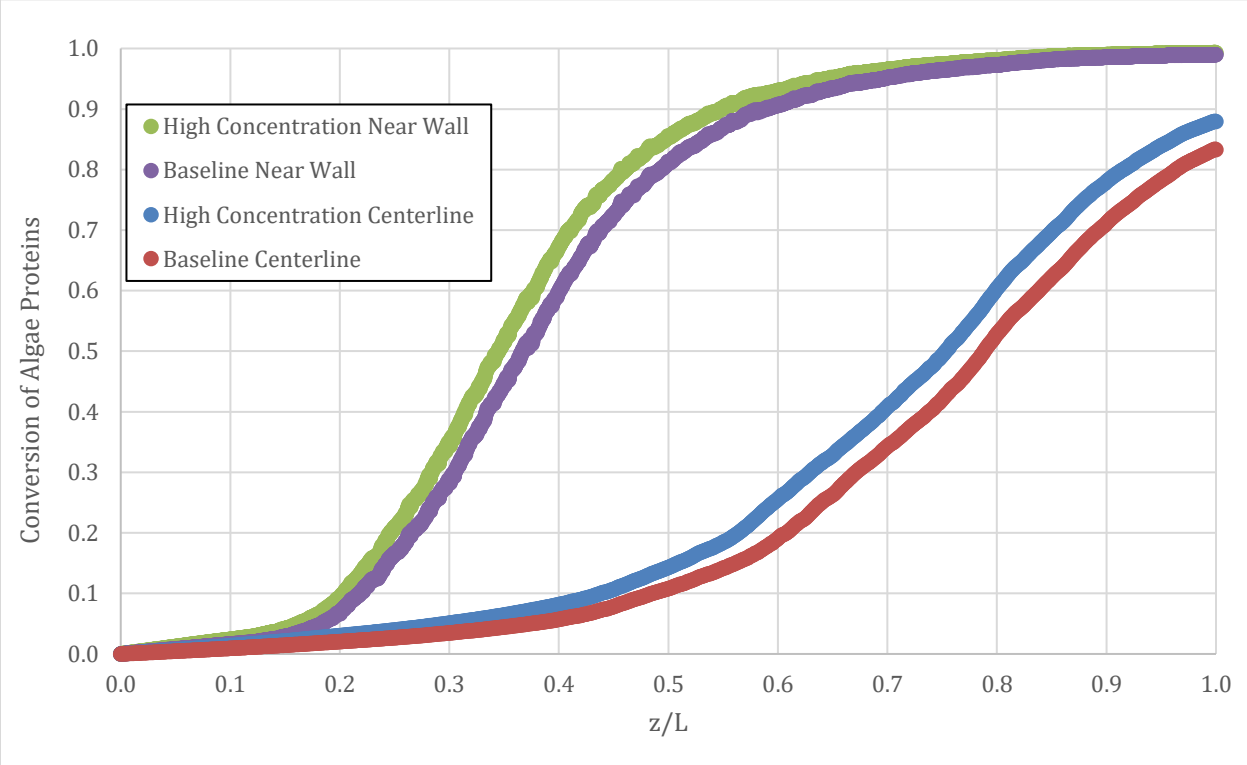

Figure 23. Comparison of conversion of proteins in the high concentration versus the baseline

The key indicator of the difference is the centerline conversion where the algae converts to soluble proteins more completely at the outlet (the right-hand limit on the x-axis). The reason for

this improvement is related to the rate equation (3), showing a quadratic dependence on algae protein concentrations. A five percent increase in the concentration of algae by mass increased the protein concentration by the same percentage and the resulting reaction achieved a higher conversion rate. This, of course, has a ceiling where the water could no longer be considered in excess and would have to factor into the rate equation. This result is encouraging for higher concentration slurries.

CHAPTER 4

CONCLUSION AND RECOMMENDATIONS FOR FUTURE WORK

The demand for green energy sources has been growing rapidly. Improved utilization of algae that creates less waste in an overall greener process is an area of potential opportunity. Although flash hydrolysis of algae has not yet achieved commercial viability, it represents a possible strategy. The Old Dominion Biomass Laboratory is experimenting with new designs for these systems which can be scaled to industrial sizes. The newly fabricated mobile pilot unit is now producing data, but the induction heating effects is not yet well understood. A COMSOL Multiphysics 5.1 reactor simulation program has been developed to better understand the reaction and guide possible opportunities for improved performance.

The model has been validated employing mass and energy balances as well as investigating sensitivity to mesh refinement studies and finally comparing simulation results with experimental test data. A baseline reaction case was simulated and validated. Seven design parameters were examined in a sensitivity analysis to detect possible design improvements. From the sensitivity analysis a reduction in reactor tube diameter was found to heat the entire flow more uniformly. Several other results proved to be noteworthy, including an increase in coil pitch heated the flow more effectively. Higher coil densities allow the slurry temperature time to equilibrate more uniformly which is preferable. Also, thinner reactor tube wall thickness enables improved induction heating efficiency lowering the power requirement.

Three-dimensional simulations could be run to examine the actual helical coil effects as well as incorporating a protruding thermocouple probe. Simulations could be run extending the conversion reactions beyond the physical reactor limit to examine residual reaction processes—

particularly how the arginine reaction proceeds. Simulating the specific algae reactions rather than assuming a lumped reaction model is more desirable. Incorporating a realistic overheating product determination is a critical need. Factorial experimentation could be used to analyze the combinations of possible design changes and formulate a numerical model for a proper optimization study. COMSOL also has a "coil geometry analysis" package and several optimization study options that could simulate different coil shapes and pitches to optimize design for this application. Possible reactor tube network geometry changes for better mixing can be considered. For now, this model serves as a functional simulation for further analysis and design iteration with the ultimate goal of proving that flash hydrolysis is feasible for industry use.

REFERENCES

[1] J. L. Garcia-Moscoso, W. Obeid, S. Kumar, and P. G. Hatcher, "Flash hydrolysis of microalgae (Scenedesmus sp.) for protein extraction and production of biofuels intermediates," *The Journal of Supercritical Fluids*, vol. 82, pp. 183-190, 2013.

[2] J. Sheehan, "Reactions of Proteins in High Temperature Water," PhD Dissertation, Dept. Chemical Engineering, Penn. State Univ., State College, USA, 2019. [Online]. Available: https://etda.libraries.psu.edu/catalog/16617jds574. [Accessed Nov. 12, 2020].

[3] N. M. Jamil, "Mathematical Modeling and Simulation of Biofuel Production from Lignocellulosic Biomass," PhD Dissertation, Dept. Math., Univ. of South Carolina, Columbia, USA, 2015. [Online]. Available: https://odu-primosb.hosted.exlibrisgroup .com/permalink/f/mkfd3u/TN_cdi_proquest_journals_1690276454. [Accessed Nov. 12, 2020].

[4] A. Álvarez-Murillo, E. Sabio, B. Ledesma, S. Román, and C. M. González-García, "Generation of biofuel from hydrothermal carbonization of cellulose. Kinetics modelling," *Energy*, vol. 94, pp. 600-608, 2016.

[5] P. Ranganathan, and S. Savithri, "Computational Fluid Dynamics simulation of hydrothermal liquefaction of microalgae in a continuous plug-flow reactor," *Bioresource technology*, vol. 258, pp. 151-157, 2018.

[6] J. L. Garcia-Moscoso, A. Teymouri, and S. Kumar, "Kinetics of peptides and arginine production from microalgae (Scenedesmus sp.) by flash hydrolysis," *Industrial & Engineering Chemistry Research*, vol. 54, no. 7, pp. 2048-2058, 2015.

[7] H. S. Fogler, "12.7 Radial and Axial Variations in a Tubular Reactor," in *Elements of Chemical Reaction Engineering,* 5th ed. Boston, MA, USA: Prentice Hall, 2016, ch.12, sec. 7, pp. 595- 602.

[8] A. Lee, D. Lewis, T. Kalaitzidis, and P. Ashman, "Technical issues in the large-scale hydrothermal liquefaction of microalgal biomass to biocrude." *Current Opinion in Biotechnology*, vol. 38, pp. 85-89, 2016.

[9] A. Asiedu, B. Stuart, E. Resurreccion, and S. Kumar, "Techno-economic analysis of protein concentrate produced by flash hydrolysis of microalgae," *Environmental Progress & Sustainable Energy*, vol. 37, no. 2, pp. 881-890, 2018.

[10] M. J. Martin, "Challenges of Designing and Operating a Pilot Scale Short Residence Time Continuous Hydrothermal Flash Hydrolysis Reactor for High Slurry Load Biomass Processing," M.S. thesis, Dept. Civil and Environ. Engineering, Old Dominion Univ., Norfolk, VA, USA, 2019.

[11] S. Solmaz, "Multiphase Flow in CFD: Basics and Modeling," *simscale.net,* Mar. 19, 2019. [Online]. Available: https://www.simscale.com/blog/2017/12/multiphase-flow/. [Accessed Nov. 12, 2020].

[12] S. Balachandar, and J. K. Eaton, "Turbulent dispersed multiphase flow," *Annual Review of Fluid Mechanics*, vol. 42, pp. 111-133, 2010.

[13] M. M. Awad, and S. N. Kazi, *Two-phase flow,* Rijeka, Croatia: InTech, 2012, pp. 251-340. [Online]. Available: https://www.intechopen.com/books/an-overview-of-heat-transfer-phenomena/two-phase-flow. [Accessed Nov. 12, 2020].

[14] R. Harun, M. K. Danquah, and S. Thiruvenkadam, "Particulate size of microalgal biomass affects hydrolysate properties and bioethanol concentration," *BioMed Research International*, 2014.

[15] Fairchild Semiconductor, *Induction Heating System Topology Review*, 2000. [Online]. Available: http://notes-application.abcelectronique.com/009/9-12623.pdf. [Accessed Nov. 12, 2020].

[16] D. Istardi, and A. Triwinarko, "Induction Heating Process Design Using COMSOL Multiphysics Software," *Telkomnika*, vol. 9, no. 2, 2011.

[17] M. W. Kennedy, "Magnetic fields and induced power in the induction heating of aluminium billets," PhD dissertation, Dept. Materials Sci. and Engineering, KTH Royal Institute of Technology, Stockholm, Sweden, 2013. [Online]. Available: https://www.diva-portal.org/smash/record.jsf?pid=diva2%3A630122&dswid=1172. [Accessed Nov. 12, 2020].

[18] F. Li, J. Ning, and S. Y. Liang, "Analytical modeling of the temperature using uniform moving heat source in planar induction heating process," *Applied Sciences*, vol. 9, no. 7, 2019.

[19] L. P. de Oliveira, D. Hudebine, D. Guillaume, and J. J. Verstraete, "A review of kinetic modeling methodologies for complex processes," *Oil & Gas Science and Technology– Revue d'IFP Energies nouvelles*, vol. 71, no. 3, 2016.

[20] "Relative Permittivity - the Dielectric Constant," *engineeringtoolbox.com,* 2010. [Online]. Available: https://www.engineeringtoolbox.com/relative-permittivity-d_1660.html. [Accessed Sept. 14, 2020].

[21] "Permeability," *engineeringtoolbox.com*, 2016. [Online]. Available: https://www.engineeringtoolbox.com/permeability-d_1923.html. [Accessed Sept. 14, 2020].

[22] C. A. Meyer, "ASME Steam Tables: Thermodynamic and Transport Properties of Steam," 6th ed., *American Society of Mechanical Engineers,* New York, NY, USA, 1993.

[23] R. Sukhon, R. Kongchana, K. Khongsiri, B. Puntaratronnugoon, and V. Tulasombut, "A study on volumetric magnetic susceptibility of weight due to its manufacturing process," presented at IMEKO TC3, TC5 and TC22 Conferences Metrology in Modern Context, Pattaya, Chonburi, Thailand, Nov. 22-25, 2010.

[24] Y. Tanaka, H. Saito, Y. Tsutsumi, H. Doi, H. Imai, and T. Hanawa, "Active hydroxyl groups on surface oxide film of titanium, 316L stainless steel, and cobalt-chromium-molybdenum alloy and its effect on the immobilization of poly (ethylene glycol)," *Materials Transactions*, vol. 49, no. 4, pp. 805-811, 2008.

[25] Y. A. Çengel, and A. J. Ghajar, "Table A-3 Properties of solid metals," In *Heat and Mass Transfer: Fundamentals & Applications.* 4th ed., New York, NY, USA: McGraw-Hill, 2012, ch. Appendix A, pp. 868-870.

[26] B.S. Mitchell, "Appendix 8: Electrical Conductivity of Selected Materials," In *An Introduction to Materials Engineering and Science*, Hoboken, NJ, USA: John Wiley & Sons, 2004 ch. Appendix 8, pp. 893.

[27] "Coefficients of Linear Thermal Expansion," *engineeringtoolbox.com*, 2003. [Online]. Available: https://www.engineeringtoolbox.com/linear-expansion-coefficients-d_95.html. [Accessed Sept. 14, 2020].

[28] "Material Properties and Physical Properties of Materials," In *2017 ASHRAE Handbook: Fundamentals: SI edition*, Atlanta, GA, USA: ASHRAE, 2017, ch. 26,33.

[29] "Thermophysical Properties of Fluid Systems," *NIST Chemistry WebBook, SRD 69*, 2018. [Online]. Available: https://webbook.nist.gov/chemistry/fluid. [Accessed Sept. 14, 2020].

[30] B. V. Babu, and A. S. Chaurasia, "Dominant design variables in pyrolysis of biomass particles of different geometries in thermally thick regime," *Chemical Engineering Science*, vol. 59, no. 3, pp. 611-622, 2004.

[31] S. C. Cheng, and R. I. Vachon, "A technique for predicting the thermal conductivity of suspensions, emulsions and porous materials," *International Journal of Heat and Mass Transfer*, vol. 13, no. 3, pp. 537-546, 1970.

[32] N. Schneider, T. J. Fortin, R. Span, and M. Gerber, "Thermophysical properties of the marine microalgae Nannochloropsis salina," *Fuel Processing Technology*, vol. 152, pp. 390-398, 2016.

[33] M. Popovic, "Thermodynamic properties of microorganisms: determination and analysis of enthalpy, entropy, and Gibbs free energy of biomass, cells and colonies of 32 microorganism species," *Heliyon*, vol. 5, no. 6, 2019.

[34] C. O. Popiel, J. Wojtkowiak, and K. Bober, "Laminar free convective heat transfer from isothermal vertical slender cylinder," *Experimental Thermal and Fluid Science*, vol. 32, no. 2, pp. 607-613, 2007.

[35] F. Bocchi, "How to Calculate Mass Conservation and Energy Balance," *comsol.com,* Oct. 14, 2015. [Online]. Available: http://www.comsol.com/blogs/how-to-calculate-mass-conservation-and-energy-balance/. [Accessed Sept. 14, 2020].

APPENDICES

A. MESH REFINEMENT DATA

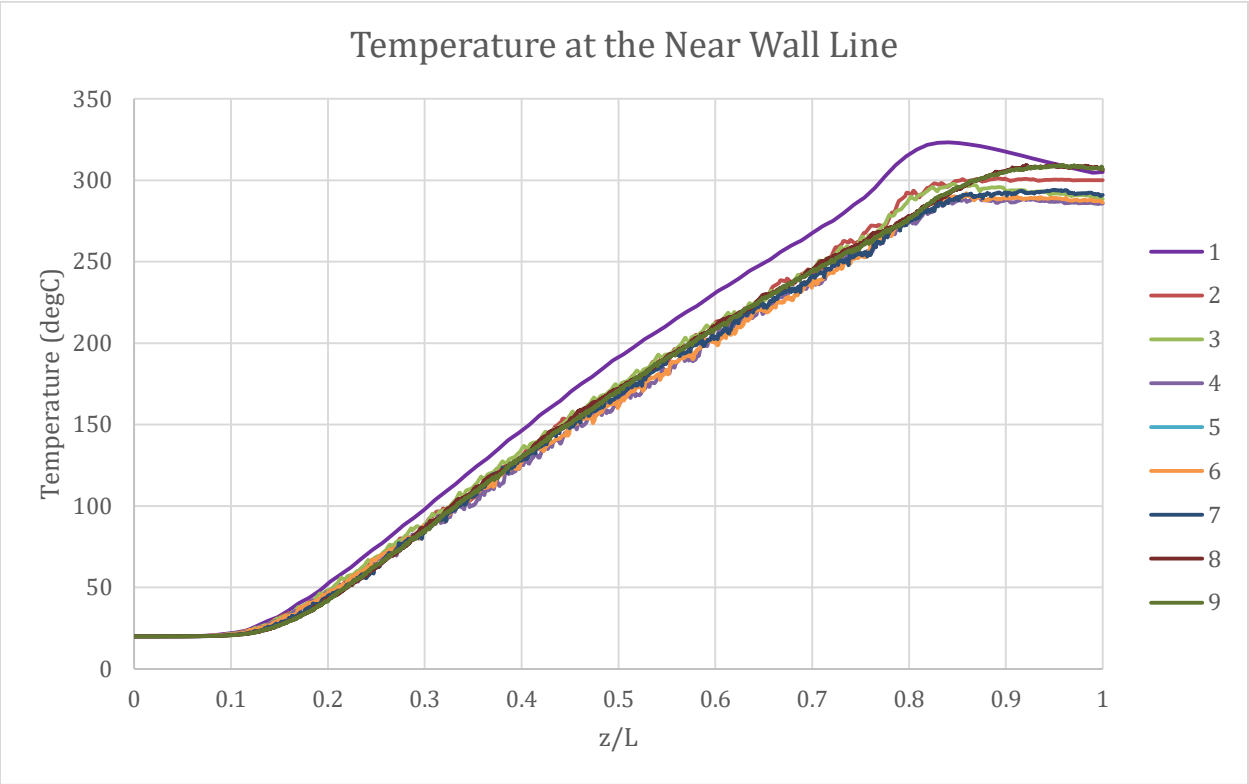

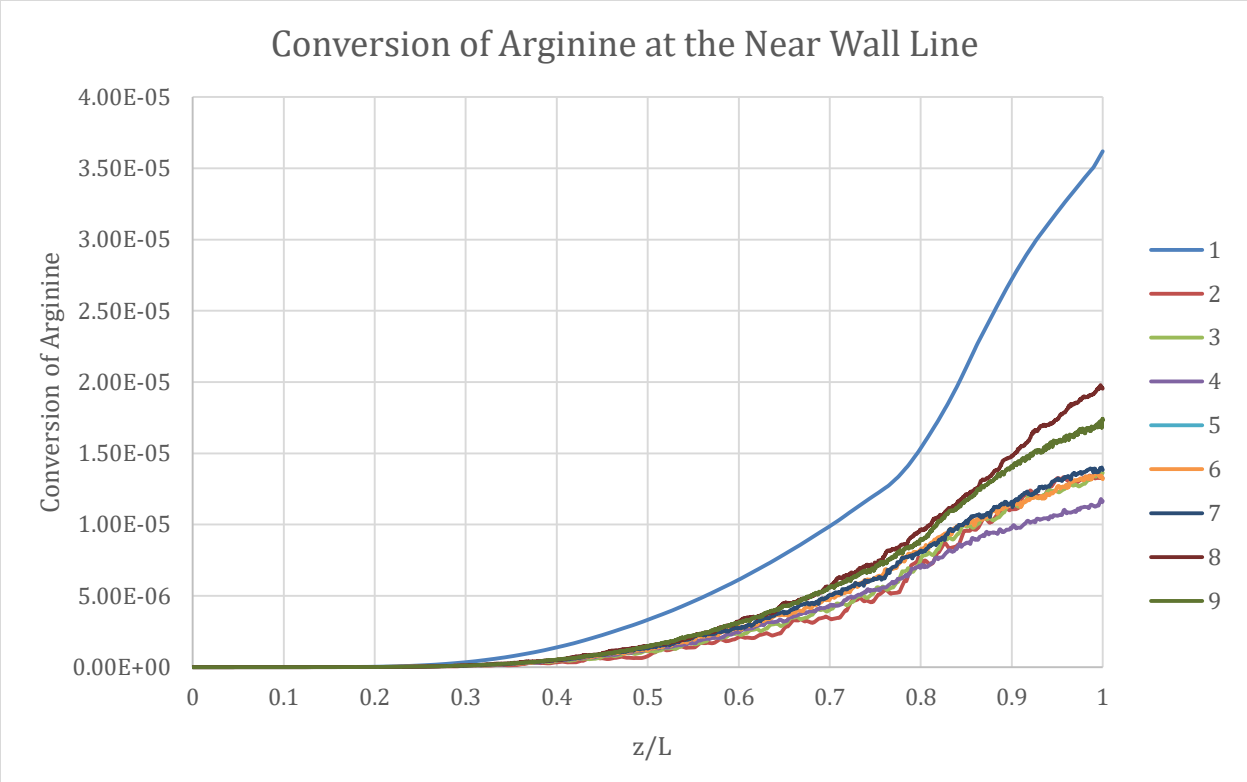

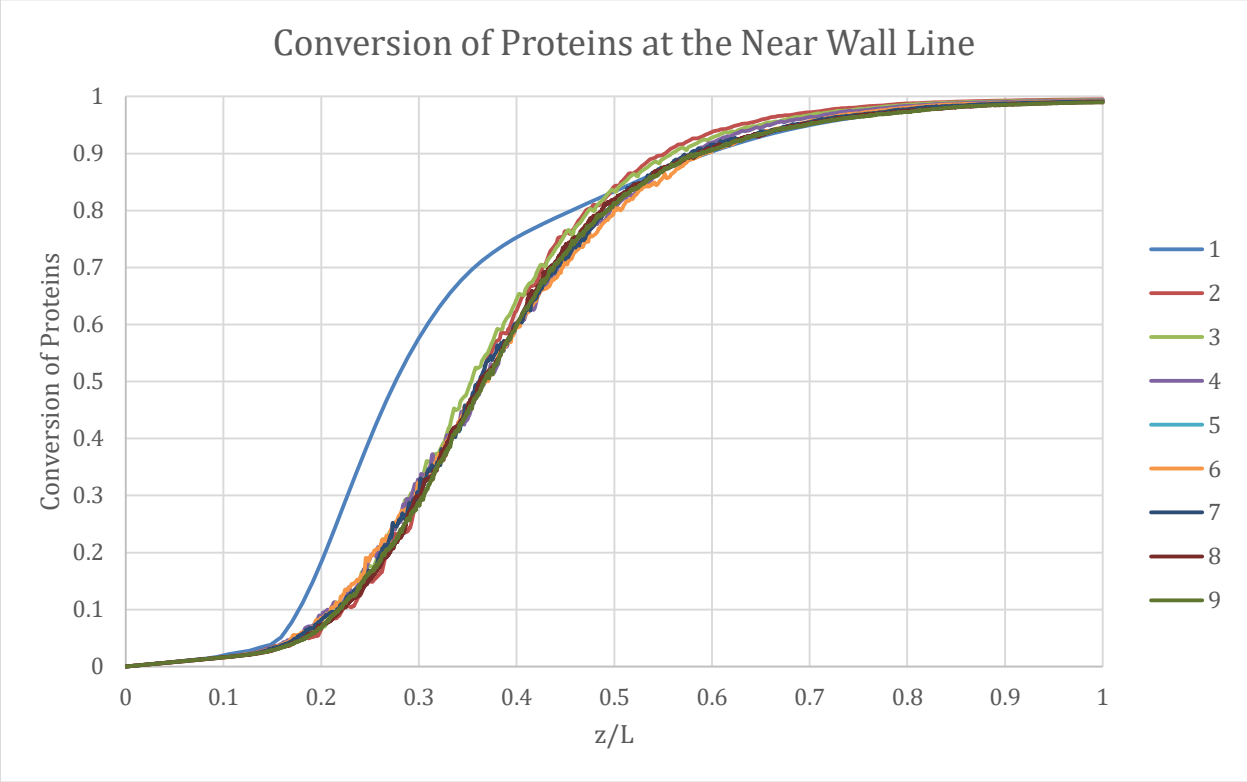

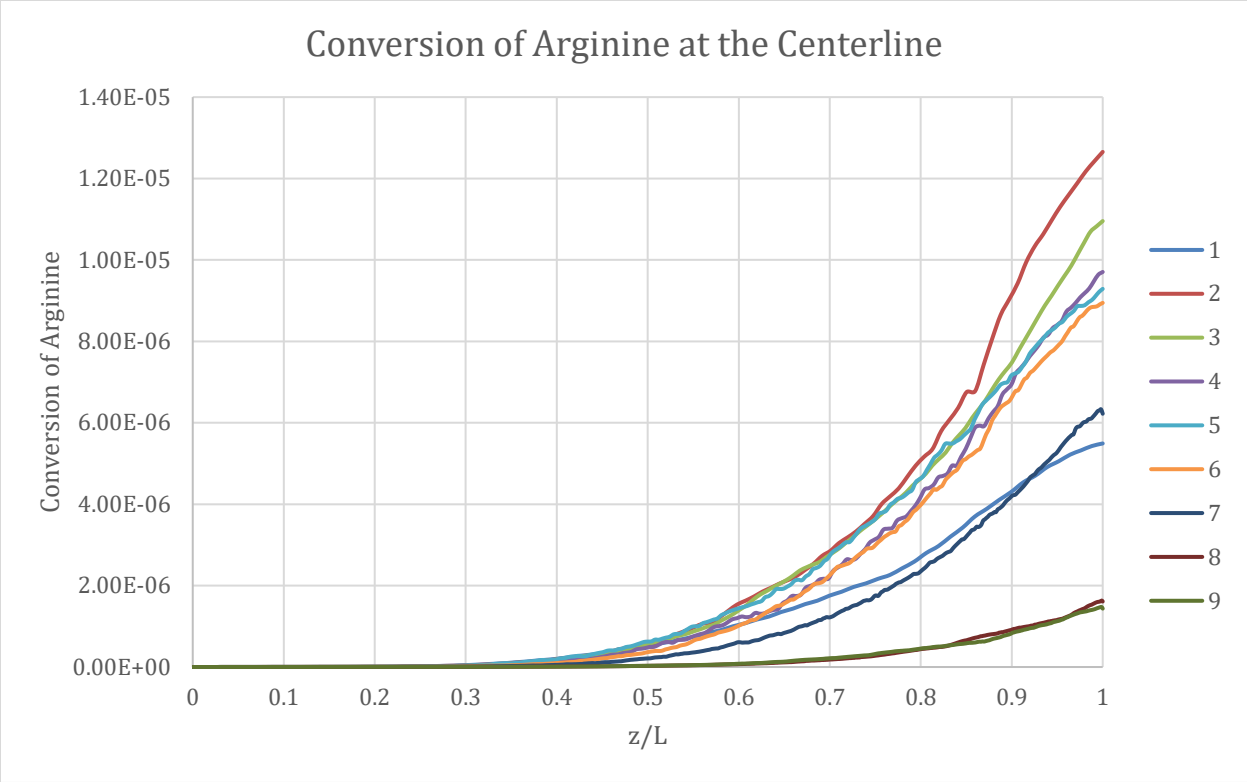

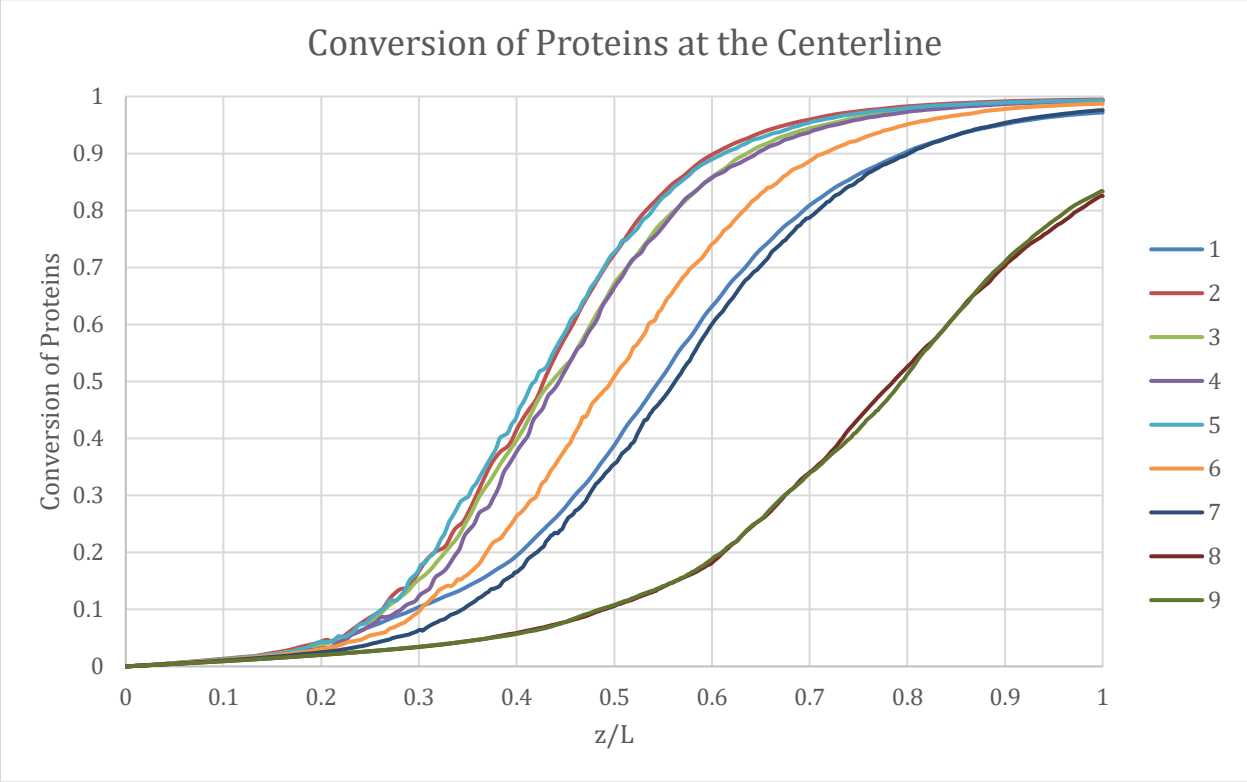

VITA

Noah Joseph LeGrand

EDUCATION

Master of Science in Mechanical Engineering

Old Dominion University, Norfolk, VA

Intended Date of Graduation: December 2020

Concentration: Thermodynamics and Energy Conversions

Bachelor of Science in Mechanical Engineering

Old Dominion University, Norfolk, VA

Date of Graduation: May 2019 Summa cum Laude

Concentration: Power/Energy Conversions

WORK EXPERIENCE

1/19-Current: Department Tutor/Teaching Assistant, Old Dominion University

9/18-12/18: Manufacturing Engineering Intern, Plasser American Corporation

5/18-8/18: Co-Op Mechanical Engineer, T. Jefferson National Accelerator Facility

5/17-5/18: Product Development/Transmission Engineer Intern, Volvo Penta of the Americas

9/16-5/17: Plastic Fabricator, Norva Plastics

INTERESTS Green energy, thermal-fluid sciences, propulsion systems, automotive, nature